

# Strong and almost strong modes of Floquet spin chains in Krylov subspaces

Daniel J. Yates and Aditi Mitra

*Center for Quantum Phenomena, Department of Physics,  
New York University, 726 Broadway, New York, NY, 10003, USA*

(Dated: November 12, 2021)

Integrable Floquet spin chains are known to host strong zero and  $\pi$  modes which are boundary operators that respectively commute and anticommute with the Floquet unitary generating stroboscopic time-evolution, in addition to anticommuting with a discrete symmetry of the Floquet unitary. Thus the existence of strong modes imply a characteristic pairing structure of the full spectrum. Weak interactions modify the strong modes to almost strong modes that almost commute or anticommute with the Floquet unitary. Manifestations of strong and almost strong modes are presented in two different Krylov subspaces. One is a Krylov subspace obtained from a Lanczos iteration that maps the time-evolution generated by the Floquet Hamiltonian onto dynamics of a single particle on a fictitious chain with nearest neighbor hopping. The second is a Krylov subspace obtained from the Arnoldi iteration that maps the time-evolution generated directly by the Floquet unitary onto dynamics of a single particle on a fictitious chain with longer range hopping. While the former Krylov subspace is sensitive to the branch of the logarithm of the Floquet unitary, the latter obtained from the Arnoldi scheme is not. The effective single particle models in the Krylov subspace are discussed, and the topological properties of the Krylov chain that ensure stable 0 and  $\pi$  modes at the boundaries are highlighted. The role of interactions is discussed. Expressions for the lifetime of the almost strong modes are derived in terms of the parameters of the Krylov subspace, and are compared with exact diagonalization.

## I. INTRODUCTION

The Kitaev chain [1], which after a Jordan-Wigner transformation maps to the transverse field Ising model (TFIM) [2], despite its apparent simplicity, is a toy model for understanding diverse phenomena such as quantum phase transitions [2] and topological systems [3]. It also forms a building block for realizing non-Abelian braiding [4–7]. In recent years, periodic or Floquet driving of this model has helped conceptualize new phenomena such as boundary and bulk discrete time crystals [8–10].

A key feature of the TFIM model, and its anisotropic generalization, is that it hosts robust edge modes known as strong zero modes (SZMs) [1, 11]. An operator  $\Psi_0$  is a SZM if it obeys certain properties. Firstly it should commute with the Hamiltonian  $H$  in the thermodynamic limit i.e,  $[\Psi_0, H] \approx 0$ , secondly it should anticommute with a discrete (say  $\mathbb{Z}_2$ ) symmetry of the Hamiltonian  $\mathcal{D}$ ,  $\{\Psi_0, \mathcal{D}\} = 0$ , and thirdly it should be a local operator with the property  $\Psi_0^2 = O(1)$ . The presence of a SZM immediately implies that the entire spectrum of  $H$  is doubly degenerate, where the degenerate pairs are  $\{|n\rangle, \Psi_0|n\rangle\}$ , with each member of the pair being eigenstates of  $\mathcal{D}$ , but in the opposite symmetry sector. This eigenstate-phase makes the edge modes extremely stable to adding symmetry preserving perturbations, such as exchange interactions between spins. In particular, the edge modes acquire a finite lifetime in the presence of interactions, but with the lifetime being non-perturbative in the strength of the interactions [12–17]. These long-lived quasi-stable modes in the presence of perturbations are referred to as almost strong zero modes (ASZMs) [13].

Under Floquet driving, besides the SZMs, new edge modes arise [18–22], which are called strong  $\pi$  modes

(SPMs) [22], with the possibility of having phases where SZMs and SPMs co-exist [22–26]. In order to define the strong modes in a Floquet system, one needs to adapt the previous definition of the SZM to that of a Floquet unitary over one drive cycle,  $U$ . The SZM  $\Psi_0$  and the SPM  $\Psi_\pi$  are now defined as follows. Both these operators anticommute with the discrete symmetry of  $U$ ,  $\{\Psi_0, \mathcal{D}\} = 0$ ,  $\{\Psi_\pi, \mathcal{D}\} = 0$ . But while the SZM  $\Psi_0$  commutes with the Floquet unitary in the thermodynamic limit  $[\Psi_0, U] \approx 0$ , the SPM  $\Psi_\pi$  anticommutes with it  $\{\Psi_\pi, U\} \approx 0$  in the same limit. Moreover, as for the static case, both operators are local, with the property  $\Psi_{0,\pi}^2 = O(1)$ . Thus existence of  $\Psi_0$  implies that the entire spectrum of  $U$  is doubly degenerate  $\{|n\rangle, \Psi_0|n\rangle\}$ , with the two eigenstates of a pair also being eigenstates of opposite symmetry. The existence of  $\Psi_\pi$  also implies that the spectrum is paired, but with each pair  $|n\rangle, \Psi_\pi|n\rangle$  not only being eigenstates of opposite symmetry, but also being separated by the quasi-energy of  $\pi/T$ , with  $T$  being the period of the drive. In particular, the eigenstate pair  $|n\rangle, \Psi_\pi|n\rangle$  pick up a relative phase of  $-1$  after odd stroboscopic time-periods. Thus the SPM is an example of a boundary time-crystal.

The Majorana mode of the Kitaev chain is an example of a SZM discussed above, but written in the Majorana basis. From the discussion above it follows that with open boundary conditions, not just the ground state, but all the eigenstates of the Kitaev chain are doubly degenerate in the topologically non-trivial phase. In a similar manner, Floquet driving the Kitaev chain gives rise to  $\pi$  Majorana modes. These are examples of the SPMs discussed above, with their existence implying a  $\pi$ -pairing for the entire spectrum of the Floquet unitary.

The strong modes are a property of the entire Hilbert space. When interactions are included in the Kitaev

chain, the SMs reduce to ASMs, i.e, the exact pairing structure of the entire Hilbert space reduces to an approximate pairing. However even with interactions, there is an integrable limit, corresponding to the XYZ chain after a Jordan-Wigner transformation, where SMs survive [11]. For a generic non-integrable chain which does not have SMs, when the interactions are weak and hence irrelevant in a renormalization group sense, one can still have zero modes that ensure a degeneracy only in the ground state sector. These zero modes are known as weak zero modes [27–29].

In the Floquet setting, SZMs and SPMs have been identified in free fermion (integrable) Floquet chains [18, 20, 22]. In addition, the effect of weak interactions was explored using exact diagonalization (ED) where it was found that quasi-stable and long lived edge modes exist despite bulk heating [22]. Drawing inspiration from the static case [13], these quasi-stable modes are called ASZMs and almost strong  $\pi$  modes (ASPMs) [22]. The current paper proposes a route to understanding these quasi-stable modes by mapping their dynamics to a Krylov subspace. A similar study was performed for ASZMs in static chains [16, 17]. In addition, a recent paper showed how the Krylov method can be generalized to Floquet systems, where the method used was a Lanczos iteration scheme based on the Floquet Hamiltonian [30]. Here we further expand on this method, and also introduce the Arnoldi method, which is based on the Floquet unitary rather than the Floquet Hamiltonian, as a promising alternate route. Since the Krylov subspace dynamics, whether generated by the Lanczos method or the Arnoldi method, is the dynamics of a free particle on a fictitious one-dimensional ( $1d$ ) lattice, the Krylov chain, this mapping paves the way for developing analytic methods to extract the lifetimes for general interacting and driven settings.

The paper is organized as follows. The integrable model is introduced in Section II, and its phases outlined. In Section III the Heisenberg time-evolution of the SZM and SPM are mapped to a Krylov subspace via a Lanczos iteration scheme where the generator of the dynamics is the logarithm of the Floquet unitary over one drive cycle, i.e., the Floquet Hamiltonian. In Section IV, the dynamics generated by the Floquet unitary is mapped to a Krylov subspace via the Arnoldi iteration [31]. In section V analytic expressions of the Krylov subspace arising from the Arnoldi method are derived in the free limit. In Section VI, the Arnoldi iteration is used to arrive at a compact expression for the lifetime of the edge modes that holds for finite size systems as well as non-zero interactions. In Section VII, the effect of interactions is discussed, and the lifetime of the edge modes obtained from Krylov space methods are compared with ED. We present our conclusions in Section VIII.

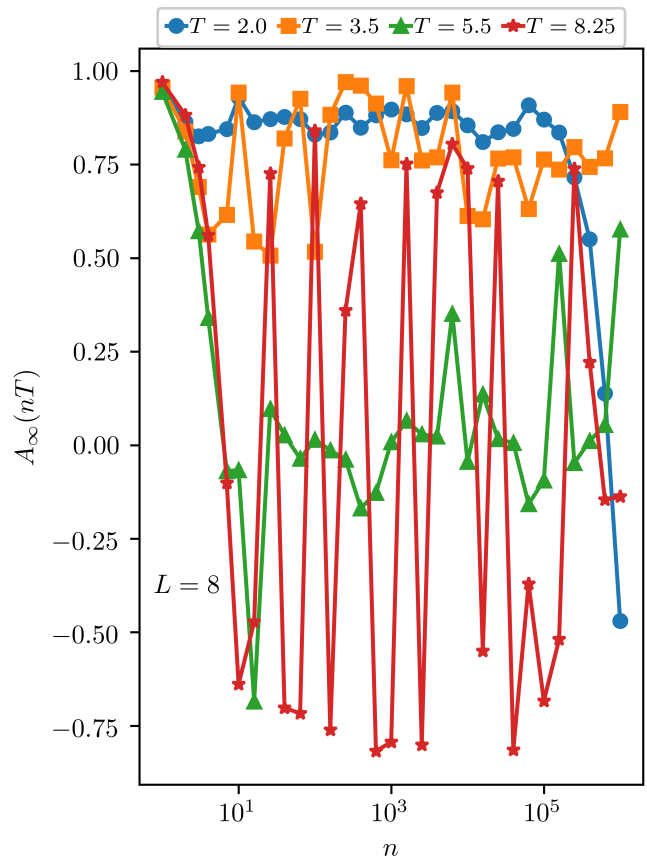


FIG. 1. The autocorrelation function  $A_\infty$  at logarithmically separated stroboscopic times for a chain of length  $L = 8$  and for the free binary drive. The parameters are  $g = 0.3$  and  $T = 2.0, 3.5, 5.5, 8.25$  corresponding respectively to SZM phase, SZM-SPM phase, trivial phase, and a SPM phase.

## II. MODEL

In this section we introduce the integrable model of the Floquet chain. We consider an open chain of length  $L$  where the stroboscopic time evolution is generated by the following Floquet unitary [20, 22, 23, 25, 32, 33]

$$U = e^{-i\frac{T}{2}J_x H_{xx}} e^{-i\frac{T}{2}gH_z}, \quad (1)$$

where

$$H_z = \sum_{i=1}^L \sigma_i^z, \quad (2)$$

$$H_{xx} = \sum_{i=1}^{L-1} \sigma_i^x \sigma_{i+1}^x. \quad (3)$$

In what follows we set  $J_x = 1$ . Eq. (1) is a binary drive where the first part of the drive involves time-evolution purely by the local magnetic field of strength  $gT$ , while the second part of the drive involves time-evolution with respect to the nearest-neighbor Ising inter-

action of strength  $T$ . The Floquet unitary has a discrete symmetry as it commutes with

$$\mathcal{D} = \sigma_1^z \dots \sigma_L^z. \quad (4)$$

When we add interactions in Section VII,  $\mathcal{D}$  will continue to be a symmetry of the problem.

When  $T \ll 1$ , a high frequency expansion gives the Floquet Hamiltonian  $H_F = H_{xx}/2 + gH_z/2$ . Moreover, in this high frequency limit,  $T$  can be interpreted as the period of the drive, with the stroboscopic time-evolution being  $U = e^{-iH_F T}$ . The phases of the Kitaev chain are recovered in the high frequency limit, where as  $g$  is tuned from  $g < 1$  to  $g > 1$ , one encounters a quantum phase transition from a topologically non-trivial phase to a topologically trivial phase. We are interested in general  $T$  where the phase diagram is much richer. Eventually we are interested in how these phases manifest in the Krylov subspace.

It is convenient to map the problem to Majorana fermions as follows

$$a_{2\ell-1} = \prod_{j=1}^{\ell-1} \sigma_j^z \sigma_\ell^x; \quad a_{2\ell} = \prod_{j=1}^{\ell-1} \sigma_j^z \sigma_\ell^y, \quad (5)$$

where  $\ell = 1 \dots L$ . Denoting the vector

$$\vec{a} = \begin{pmatrix} a_1 \\ a_2 \\ a_3 \\ \vdots \\ a_{2L} \end{pmatrix}, \quad (6)$$

the stroboscopic time-evolution of  $\vec{a}$  is as follows

$$U^\dagger \vec{a} U = K \vec{a}, \quad (7)$$

where on defining

$$c_1 = \cos(Tg), \quad (8a)$$

$$c_2 = \cos(T), \quad (8b)$$

$$s_1 = \sin(Tg), \quad (8c)$$

$$s_2 = \sin(T), \quad (8d)$$

we find that  $K$  takes the following form [22] for  $L = 3$

$$K = \begin{pmatrix} c_1 & -s_1 & 0 & 0 & 0 & 0 \\ s_1 c_2 & c_1 c_2 & -c_1 s_2 & s_1 s_2 & 0 & 0 \\ s_1 s_2 & c_1 s_2 & c_1 c_2 & -s_1 c_2 & 0 & 0 \\ 0 & 0 & s_1 c_2 & c_1 c_2 & -c_1 s_2 & s_1 s_2 \\ 0 & 0 & s_1 s_2 & c_1 s_2 & c_1 c_2 & -s_1 c_2 \\ 0 & 0 & 0 & 0 & s_1 & c_1 \end{pmatrix}. \quad (9)$$

$K$  is an orthogonal matrix which, depending on the parameters can admit eigenvalues at  $\pm 1$ . While  $K$  has been shown explicitly for  $L = 3$ , the form for general  $L$  can be easily guessed as the bulk consisting of the second and third rows are repeated. For the example of  $L = 3$  given above, we see that the bulk structure is repeated twice.

A key quantity that we will analyze is the autocorrelation function of  $\sigma_1^x = a_1$ , evaluated at stroboscopic times

$$A_\infty(nT) = \frac{1}{2L} \text{Tr} \left[ \sigma_1^x(nT) \sigma_1^x(0) \right], \quad (10a)$$

$$\sigma^x(nT) = [U^\dagger]^n \sigma_1^x U^n. \quad (10b)$$

When strong modes exist, this quantity has a non-zero overlap with them, and therefore its stroboscopic time-evolution is a diagnostic for whether strong modes exist or not. This point will be further clarified below when we discuss some exactly solvable limits. Moreover, from Eq. (7) it is clear that the above autocorrelation function is completely determined by the action of  $K$  on an initial vector that is localized on the first site. Thus  $\pm 1$  eigenvalues of  $K$  imply SZMs and SPMs respectively.

We now discuss some exactly solvable limits where  $\sigma_1^x$  is the strong mode, or has an  $O(1)$  overlap with it. Below  $n$  is an integer.

- $Tg = (2n+1)\pi$ ,  $T$  arbitrary: We have  $e^{-iTgH_z/2} \propto \mathcal{D}$ , thus  $U^\dagger \sigma_1^x U = \mathcal{D} \sigma_1^x \mathcal{D} = -\sigma_1^x$ , and a SPM exists. There is however no SZM.
- $Tg = (2n)\pi$ ,  $T$  arbitrary: Now  $e^{-iTgH_z/2} \propto 1$ , thus  $U^\dagger \sigma_1^x U = \sigma_1^x$ . We now have a SZM while there is no SPM.
- $T = (2n+1)\pi$ ,  $Tg$  arbitrary: Now we have  $e^{-iTH_{xx}/2} \propto \sigma_1^x \sigma_L^x$ . With  $e^{-iTgH_z/2} = \prod_{l=1}^L [\cos(Tg/2) - i\sigma_l^z \sin(Tg/2)]$ . It is straightforward to check that

$$\begin{aligned} U^\dagger \sigma_1^x U &= \cos(Tg) \sigma_1^x - \sin(Tg) \sigma_1^y, \\ U^\dagger \sigma_1^y U &= -\sin(Tg) \sigma_1^x - \cos(Tg) \sigma_1^y. \end{aligned} \quad (11)$$

The above linear combinations of  $\sigma_1^x$  and  $\sigma_1^y$  yield a SZM and a SPM.

- $T = 2n\pi$ ,  $Tg$  arbitrary: We have  $e^{-iTH_{xx}/2} \propto 1$ . Then,

$$\begin{aligned} U^\dagger \sigma_1^x U &= \cos(Tg) \sigma_1^x - \sin(Tg) \sigma_1^y, \\ U^\dagger \sigma_1^y U &= \sin(Tg) \sigma_1^x + \cos(Tg) \sigma_1^y. \end{aligned} \quad (12)$$

The above linear combinations do not yield any strong modes unless  $Tg = m\pi$  where  $m$  is any integer. Here two cases arise depending on whether  $m$  is even or odd. If  $Tg = 2m\pi$  then  $\sigma_1^x$  is trivially a SZM because  $U \propto 1$ . If  $Tg = (2m+1)\pi$ , then  $\sigma_1^x$  is a SPM because  $U \propto \mathcal{D}$ .

The above examples show that whenever a SPM exists, the Floquet unitary has a characteristic non-local structure by either being of the form  $U \propto \mathcal{D}$  (SPM phase) or being of the form  $U \propto \sigma_1^x \sigma_L^x$  (SZM-SPM phase) [23–26]. We will show later that this non-local structure will have implications on the Krylov subspace.

The above phases are stable to perturbing around it. Fig. 1 shows  $A_\infty$  for some special cases for stroboscopic and logarithmically separated times. The parameters chosen are  $g = 0.3$ , and  $T = 2.0, 3.5, 5.5, 8.25$ . We will work with these parameters for the rest of the paper when presenting the numerical results. Among the chosen parameters, all of them except  $T = 5.5$  host strong modes. Thus for all parameters except  $T = 5.5$ ,  $A_\infty$  is long-lived with its lifetime only set by the system size  $L$ . Among these different cases,  $T = 2.0$  is a phase that has a SZM,  $T = 3.5$  is a phase that simultaneously hosts a SZM and a SPM, while  $T = 8.25$  hosts a SPM. For a SPM, the stroboscopic time-evolution flips between  $O(1)$  positive and negative values, consistent with period-doubled dynamics.

When both SZM and SPM exist,  $\sigma_1^x$  has an overlap with both of them. Thus we can write,  $\Psi_0 = a\sigma_1^x + \dots$  and  $\Psi_\pi = b\sigma_1^x(-1)^n + \dots$  where  $a, b = O(1)$  and positive  $a, b > 0$ . After the initial transients, we can write the form of  $\sigma_1^x(t)$  as  $\sigma_1^x(t) \approx c_0\Psi_0 + c_\pi\Psi_\pi + \dots$ , where  $c_{0,\pi} \leq 1/2$  for normalization. Thus the autocorrelation function becomes  $A_\infty(nT) \approx c_0a + c_\pi b(-1)^n$ . This shows that the signal will oscillate between  $c_0a + c_\pi b$  and  $c_0a - c_\pi b$ . There are several indications that  $c_0 > c_\pi$ . Firstly, note from Fig. 1 that when only a SZM is present,  $c_0 \approx 1$ , while when only a SPM is present  $c_\pi \approx 0.75$ . This is further corroborated at the exactly solvable limit for the SZM-SPM phase discussed in Eq. (11). Here one finds that at odd stroboscopic times  $A_\infty(n=1) = \cos(gT)$ , while at even stroboscopic times  $A_\infty(n=2) = 1$ . Since  $c_0 > c_\pi$ , the signal oscillates between two positive numbers, as shown in Fig. 1.

Let us define the Floquet Hamiltonian  $H_F$  as

$$H_F = \frac{i}{T} \ln(U). \quad (13)$$

Note that for the binary drive in Eq. (1), since the problem is free, the matrix  $K$  in Eq. (7) and  $U$  are simultaneously diagonalized. Thus  $i \ln K$  directly gives us the Floquet Hamiltonian  $H_F$  in the Majorana basis.

The structure of  $\ln K$  in the vicinity of some exactly solvable points was discussed in Ref. 30. In particular it was shown that when  $T \ll 1$ , and  $|gT - \pi| \ll 1$ , i.e., parameters for which the system hosts a SPM,  $i \ln K$  has the form of a topologically non-trivial Su-Schrieffer-Heeger (SSH) model [34, 35], upto an overall diagonal matrix  $\pi$ . Thus the energy of the zero mode of the SSH model is shifted by  $\pi$ , giving a SPM. Moreover, such an interpretation survived even when one tuned away from this exactly solvable limit. Ref. 30 also showed that an interpretation of the strong modes in terms of boundary modes of generalized SSH models, also survive in the Krylov subspace constructed from the Lanczos method. We will further expand on this point below, and also discuss the appearance of SSH-type chains in the Krylov subspace constructed from the Arnoldi method.

### III. KRYLOV CHAIN FROM THE LANCZOS ITERATION

The time evolution of an operator in a generic integrable or non-integrable system can be mapped to single particle dynamics on a semi-infinite chain employing a recursive Lanczos scheme [36]. This method has made a reappearance recently as a way to identify chaotic dynamics [37–40]. In this section we outline this method. The exponential complexity of solving the dynamics enters into the calculation of the hopping parameters on this chain which we denote by  $b_n$ .

Note the definition of the Floquet Hamiltonian  $H_F$  in Eq. (13). The stroboscopic time-evolution after  $m$  periods can be written in terms of  $H_F$  as follows

$$[U^\dagger]^m O U^m = e^{iH_F m T} O e^{-iH_F m T} = \sum_{n=0}^{\infty} \frac{(imT)^n}{n!} \mathcal{L}^n O, \quad (14)$$

where we define

$$\mathcal{L}O = [H_F, O]. \quad (15)$$

To employ the Lanczos algorithm, we recast the operator dynamics into vector dynamics by defining  $|O\rangle = O$ . Since we are concerned with infinite temperature quantities, we have an unambiguous choice for an inner product on the level of the operators,

$$\langle A|B\rangle = \frac{1}{2L} \text{Tr} [A^\dagger B]. \quad (16)$$

The Lanczos algorithm iteratively finds the operator basis that tri-diagonalizes  $\mathcal{L}$ . We begin with the seed “state”,  $|O_1\rangle$ , and let  $\mathcal{L}|O_1\rangle = b_1|O_2\rangle$ , where  $b_1 = \sqrt{|\mathcal{L}|O_1\rangle|^2}$ . The recursive definition for the basis operators  $|O_{n \geq 2}\rangle$  is,

$$\mathcal{L}|O_n\rangle = b_n|O_{n+1}\rangle + b_{n-1}|O_{n-1}\rangle, \quad (17)$$

where we define  $b_{n \geq 2} = \sqrt{|\mathcal{L}|O_n\rangle - b_{n-1}|O_{n-1}\rangle|^2}$ . It is straightforward algebra to check that the above procedure will iteratively find basis operators that yield a  $\mathcal{L}$  which is tri-diagonal, and of the following form,

$$\mathcal{L} = \begin{pmatrix} & b_1 & & & \\ b_1 & & b_2 & & \\ & b_2 & & \ddots & \\ & & & \ddots & \\ & & & & \ddots \end{pmatrix}. \quad (18)$$

This basis spanned by  $|O_n\rangle$  lies within the Krylov subspace of  $\mathcal{L}$  and  $|O_1\rangle$ . We refer to this tri-diagonal matrix as the Krylov Hamiltonian  $H_K$ ,

$$H_K = \sum_n b_n (c_n^\dagger c_{n+1} + c_{n+1}^\dagger c_n), \quad (19)$$

and the  $1d$  lattice it represents, the Krylov chain.

An important aspect of this technique, often overlooked when discussing chaos, is that the values of  $b_n$  are highly dependent on the choice of seed operator. Further, outside of special cases, namely a Hamiltonian that is free, the exact solution to the operation  $\mathcal{L}|O_n\rangle$  will require ED, or similar methods with equivalent costs. This method does not escape the rapidly growing exponential wall of complexity. In cases where the calculation of all  $b_n$  are possible, the above algorithm will return a value of  $b_{\text{end}} = 0$  for the very last  $b_n$ . If the iteration is continued further, all the previous  $b_n$ s will be repeated until  $b_{\text{end}} = 0$  is again reached.

For free systems, the operation  $\mathcal{L}|O_n\rangle$  can be efficiently solved when in the Majorana basis. If the starting operator is a single Majorana then the dimension of the Krylov subspace of that operator will scale as  $2L$ , as free system dynamics can only mix the individual Majoranas among themselves. Outside of free problems, the size of the full set of  $|O_n\rangle$  will be large. For example, a system size of  $L$  will have  $\sim 2^{2L}$  possible basis operators. For all intents and purposes we treat  $\mathcal{L}$  as a semi-infinite chain. If the number of solved  $b_n$  is insufficient for the quantity of interest, an approach that works well is to supplement the known set with approximate  $b_n$  that are calculated based off of trends established among the known hoppings [16, 17].

Starting with the seed state  $|O_1\rangle = |\sigma_1^x\rangle$ , we can recast  $A_\infty$  into the following form

$$A_\infty(nT) = (e^{i\mathcal{L}nT})_{1,1}. \quad (20)$$

Now, following the above discussion, the dynamics of  $A_\infty$  has been transformed into that of a semi-infinite single-particle problem. The details of the semi-infinite chain will be discussed in subsequent sections. Ref. 16 showed that the slow dynamics of  $A_\infty$  for static spin chains was a result of topological modes residing at the left boundary (origin) of the Krylov chain. We discuss the analogous situation for the Floquet problem.

Since for the binary drive, the problem is free, the matrix  $K$  in Eq. (7) and  $U$  are simultaneously diagonalized. Thus we construct the Krylov Hamiltonian by taking the Floquet Hamiltonian to be  $TH_F = i \ln(K)$  and performing the iterative steps outlined above. The parameters  $b_n$  of the Krylov Hamiltonian, and the corresponding spectra are shown in Fig. 2. The eigenfunctions with eigenvalues corresponding to 0 and  $\pm\pi$  are shown in Fig. 3.

Fig. 2 clearly shows that the Krylov chain has a dimerized structure like that of a SSH chain. The case of the SZM phase at  $T = 2.0$  and the trivial phase at  $T = 5.5$  are the easiest to understand as these correspond to SSH chains of opposite sign of the dimerization, one sign being topologically trivial ( $T = 5.5$ , with  $b_{\text{odd}} > b_{\text{even}}$ ) and the other being topologically non-trivial ( $T = 2.0$  with  $b_{\text{odd}} < b_{\text{even}}$ ). For the case of the SPM at  $T = 8.25$  (discussed in detail in Ref. 30), one finds that the very first hopping is pinned at a large value of  $O(\pi)$ , while the rest of the chain, from  $n \geq 4$  onwards has a topologically non-trivial dimerization, implying an edge mode.

The local strong hopping at the first site results in an edge mode that is pinned at  $\pm\pi$ . Thus  $\pi$  modes of the Floquet chain appear as regular zero modes of the topologically non-trivial Krylov chain with an overall shift in energy by  $\pi$  due to boundary conditions imposed by the hoppings on the first few sites. For the more complicated SZM-SPM phase at  $T = 3.5$ , the first two sites at the edges act as a two-level system that can host a pair of edge modes. These modes act as the boundary of an SSH chain with non-trivial sign of the dimerization. This point will be demonstrated further when we discuss the Krylov Hamiltonian obtained from the Arnoldi method. Also note that all the eigenvalues of  $H_K$  (lower panels of Fig. 2) lie within the Floquet Brillouin Zone (FBZ) defined as  $\epsilon T \in [-\pi, \pi]$ . However, this outcome is not guaranteed, and as we will discuss in detail later, a different basis choice can lead to an unfolded spectrum for the Krylov chain.

Fig. 3 plots the mod-square of modes at 0 and  $\pm\pi$  energies ( $|\psi_{0,\pi}(n)|^2$ ) for all the phases. Note that these modes appear in pairs in that, when a zero edge mode exists, there are two of them (orange and blue lines in the upper panels of the plot). While when a  $\pi$  mode exists, there are a pair of them located at  $\pi$  and  $-\pi$  (orange and blue lines in the lower panels of the plot). The periodicity of the spectrum under Floquet driving implies that the  $\pi$  modes are doubly degenerate in the same way as the 0 modes are because  $-\pi = \pi + 2\pi n$ , where  $n$  is any integer.

Fig. 3 shows that the degenerate pairs of edge modes are not symmetrically localized on the two ends of the Krylov chain as the chain is constructed for the operator  $\sigma_1^x$ , and is therefore heavily weighted on the left edge. If the seed operator would have been a symmetric linear combination of operators on the first and the last site of the physical chain, then the edge modes of the Krylov chain would also have been symmetrically located at the two ends of the chain. However it is interesting to note that the  $\pi$  edge mode pairs are a lot more asymmetric than the 0 edge mode pairs, where for the latter one does see two peaks, one each on the left and right edges of the Krylov chain. In contrast the  $\pi$  edge mode pairs are strongly peaked at the left edge. This is because of the highly non-local structure of the Floquet unitary when a  $\pi$  mode exists. Recall that in the previous section we showed that when a SPM exists, the Floquet unitary is proportional to the non-local operators  $\mathcal{D}$  (SPM phase) or  $\sigma_1^x \sigma_L^x$  (SZM-SPM phase), and therefore has weight on both ends of the physical chain. Thus the very first Lanczos step, even when it starts out with an operator localized at the left edge, does end up “seeing” the right end of the chain, resulting in the manifestation of the right edge mode on the left edge of the Krylov chain.

### A. Majorana basis vs spin basis

Since the Floquet Hamiltonian can always be modified by shifting the quasi-energies by integer multiples of

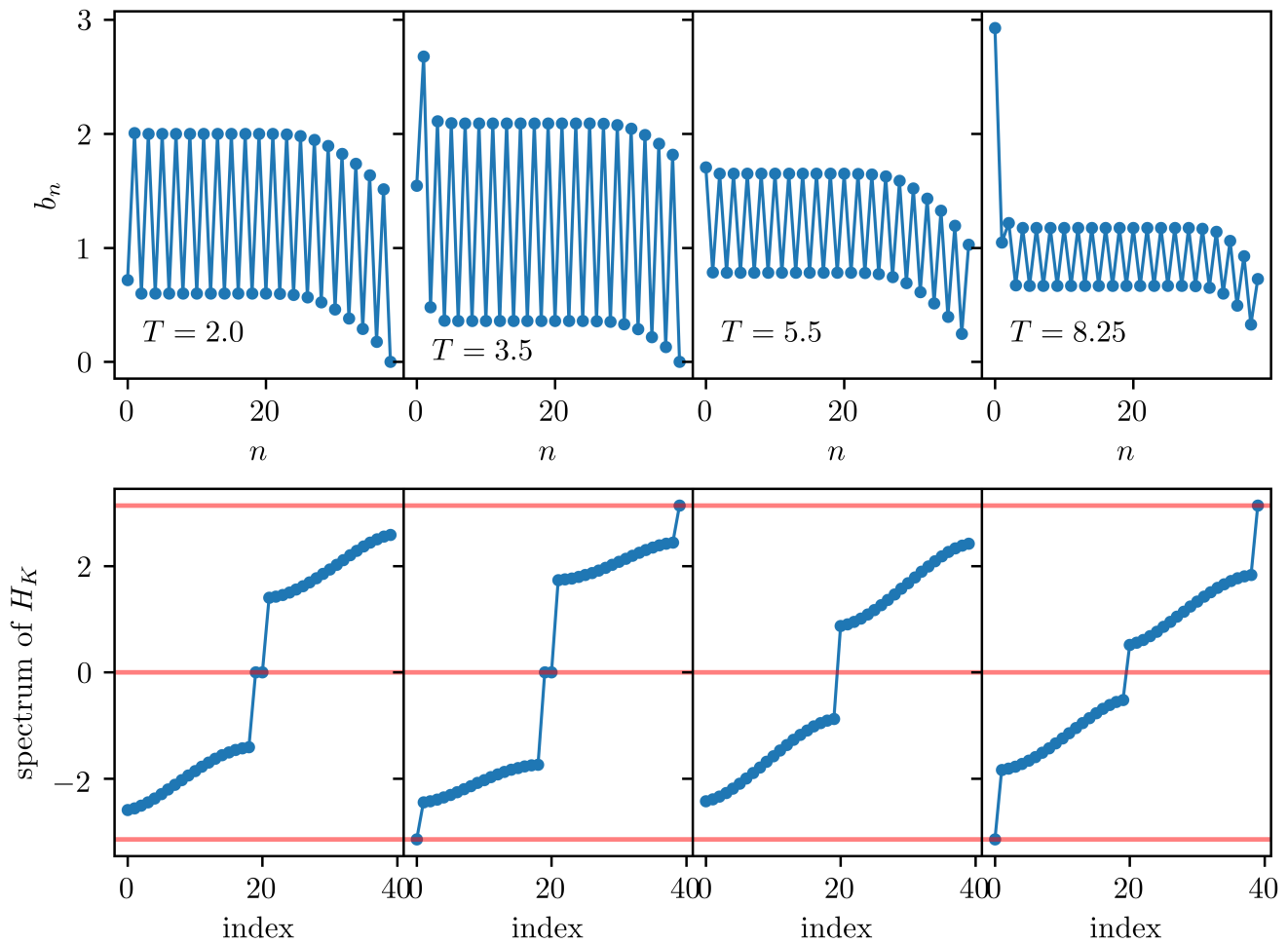


FIG. 2. Upper panel: The  $b_n$ s for the binary drive with  $g = 0.3$  and system size  $L = 20$ . Lower panel: The corresponding spectra with  $x$ -axis label “index” denoting the location of the eigenvalues arranged in ascending order. For both upper and lower panels, from left to right  $T = 2.0, 3.5, 5.5, 8.25$ . These parameters correspond to SZM, SZM-SPM, trivial, and SPM phases respectively. Horizontal red lines in lower panels correspond to energies  $0$  and  $\pm\pi$  in units of  $T^{-1}$ .

$2\pi$ , such shifts lead to different Krylov Hamiltonians, but ultimately the same physics. In this section we discuss this aspect in detail using the binary drive as an example. This issue was also discussed in Ref. 30, both for the binary drive and the interacting ternary drive, and it was pointed out that a particular choice of branchcut for  $\ln(U)$  gives a Krylov Hamiltonian that is more easy to interpret. This particular choice is one where all the quasi-energies  $\epsilon$  lie within the FBZ defined by  $\epsilon T \in [-\pi, \pi]$ .

We now discuss different ways to construct the Krylov Hamiltonian for the binary drive. One is working in the Majorana basis, and the second is working in the spin basis. Moreover, working in the spin basis, we will discuss two different Krylov chains, one where the spectrum is unfolded, while the other where the spectrum is folded into the FBZ. Note that in the Majorana basis, the spectrum is already naturally folded in the FBZ. This is because we have direct access to the orthogonal matrix  $K$

whose eigenvalues are pure phases. Moreover, the eigenvalues of the Krylov Hamiltonian in the Majorana basis equal those of  $i \ln K$ . With a choice of branchcut of the logarithm along  $(-\infty, 0)$ , this gives a spectrum for the Krylov Hamiltonian that is bounded in the FBZ.

Fig. 4 constructs the Krylov Hamiltonian for the binary drive in a few different ways. The first method is to work in the Majorana basis and to use the Lanczos method where the generator of stroboscopic dynamics is  $i \ln K$ , with  $K$  given in Eq. (9). For this case, the Lanczos method is a simple basis rotation and the spectrum of the Krylov Hamiltonian  $H_K$ , will be exactly the same as that of  $i \ln K$ . That is, we begin with a single-particle propagator  $i \ln K$ , and we end with a single-particle propagator  $\mathcal{L}$ . The orange data labeled as “free” in Fig. 4 corresponds to this case where all the computations are performed in the Majorana basis. The top panels of Fig. 4 shows the hopping parameters obtained from this procedure, and these are identical to the top panels of Fig. 2.

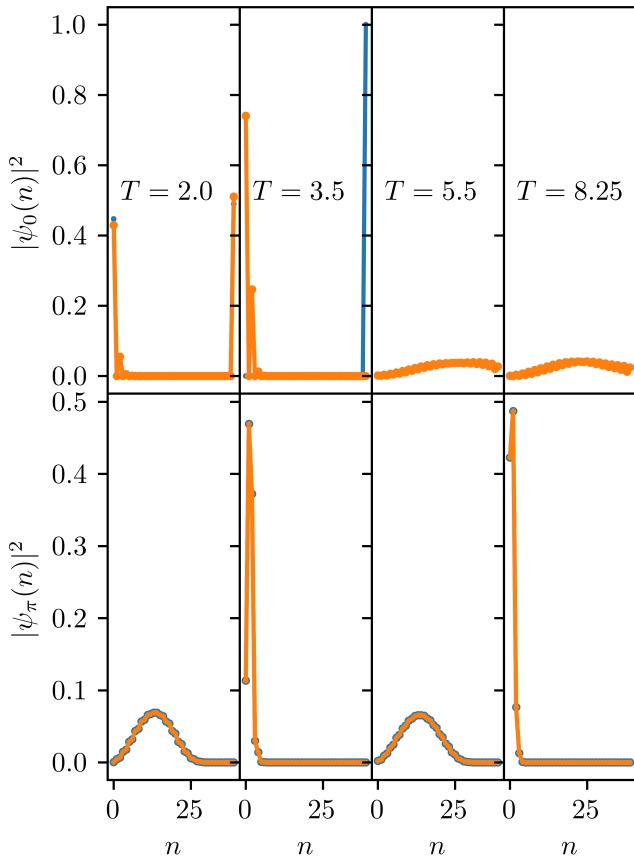


FIG. 3. The mod-square of the eigenfunctions of the Krylov chain for the same parameters as Fig. 2. Upper (lower) panels correspond to modes at zero ( $\pm\pi$ ) energy. The orange and blue data sets in each panel reflect the fact that these modes appear in pairs. In particular, there are two zero edge modes and two  $\pi$  edge modes, the latter occurring at  $\pm\pi$  energy. The plots show that  $T = 5.5$  hosts no edge modes, consistent with a trivial phase. On the other hand  $T = 2.0$  hosts a pair of edge modes at zero and no edge modes at  $\pi$  energy.  $T = 8.25$  hosts a pair of edge modes at  $\pm\pi$  but no edge modes at 0 energy.  $T = 3.5$  hosts edge modes at both 0 and  $\pm\pi$  energies.

The middle panels show the corresponding spectra and are identical to the lower panels of Fig. 2. Note that for a system size of  $L$ , the Hilbert space is exhausted at  $2L$  in the Majorana basis. We are working with a system size of  $L = 4$ . Hence top panels show orange data that correspond to a total of  $2L - 1 = 7$  hoppings, while middle panels show  $2L = 8$  eigenvalues. The lower panels show  $A_\infty$  as defined in Eq. (20) for this Krylov Hamiltonian. They agree perfectly with the ED calculation (the orange data is masked by the ED data in the lower panels).

The second way to perform the Lanczos iteration is to work in the many-body or spin basis, even though the problem is free. In this case, we are concerned with the branch of the many-body Floquet Hamiltonian  $i \ln U$ , and not of the single-particle Hamiltonian  $i \ln K$ . In Fig. 4, the blue data set labeled as “spin<sub>1</sub>” corresponds to

Lanczos performed with  $TH_F = i \ln U$  without any special treatment for the single-particle status of the problem. The seed state is  $\sigma_1^x$ . We see that the resulting spectrum of  $H_K$  in the middle panel extends beyond the FBZ as indicated by the horizontal red lines which pass through energies  $\pm\pi$ . The  $b_n$  are shown in the top row and share little in common with the  $b_n$  from the Majorana or free basis (orange crosses). The main differences between the blue data and the orange data is as follows: the spectrum is unfolded for the former and folded for the latter. Secondly, the former shows 3 gaps (at  $\epsilon T = 0, \pi, -\pi$ ), while the latter shows only two gaps ( $\epsilon T = 0, \pi$  with  $\pi$  continuously connected to  $-\pi$ ). This difference is due to the fact that the blue data does not have information regarding the periodicity of  $U$ , and so the gaps at  $\pi$  and  $-\pi$  appear to be distinct. The orange data has information about the periodicity of the spectrum as it is obtained from the exact  $K$ . Despite these differences, both Krylov Hamiltonians generate identical autocorrelation functions, as can be seen in the lower panels of Fig. 4.

We now wrap the blue spectrum of  $H_K$  such that it fits within the FBZ. This is now given by the green data set labeled “spin<sub>2</sub>” in the middle panels. This folding requires transforming the Krylov Hamiltonian as follows [30]  $H_K \rightarrow U_K \hat{\epsilon}_{\text{FBZ}} U_K^\dagger$ , where  $\hat{\epsilon}_{\text{FBZ}}$  is a diagonal matrix where all the energies lie in the FBZ, and  $U_K$  is the unitary matrix that diagonalizes  $H_K$  before the folding. After this folding, the Krylov Hamiltonian is no longer tri-diagonal, and one needs to perform a second Lanczos iteration to return to a tri-diagonal Krylov subspace. The resulting  $b_n$  of this new  $H_K$  are shown in the top panel in green, and are labeled as “spin<sub>2</sub>”. We note that this wrapping of the spectrum requires us to fully diagonalize the problem, which will typically not be possible for us when dealing with large system sizes. We see that the green  $b_n$  of the top row match the  $b_n$  obtained from the single-particle Majorana basis upto  $b_{n=2L-1}$ . At  $n = 2L$ ,  $b_{2L} = 0$  so that all the  $b_n$  appearing after that represent a second chain decoupled from the part that lies between  $n = 1 \dots 2L - 1$ . The significance of these decoupled chains on the spectrum is shown in the middle panels (green data). Here we see that the spectrum is repeated twice for our example. This repetition does not influence the physics, as can be seen in the lower panel which plots  $A_\infty$ . This is because once  $b_m = 0$ , the remaining  $b_{n>m}$  do not affect the dynamics. The bottom panel in Fig. 4 plots  $A_\infty$  for the Krylov Hamiltonian obtained after the folding. The results agree perfectly with ED, and the two other Krylov Hamiltonians discussed previously.

Thus while the  $b_n$  and the spectra (top and center rows of Fig. 4) are sensitive to whether the Lanczos is performed on the level of the many-body or spin basis versus the single-particle or Majorana basis, the dynamics is not sensitive to it. As touched upon in the previous paragraph, to align the Majorana picture and the spin picture, we needed to wrap the spectrum of  $H_K$ , requiring the full diagonalization of  $H_K$ . This is only possible in

the free case where we can easily find the full Krylov subspace of the seed operator. Moreover, the reason for the very different  $b_n$ s in the spin and in the Majorana bases, arises due to the ambiguity associated with the branch of  $H_F = i \ln(U)/T$ . To avoid this ambiguity, it is better to set up the problem in an alternate Krylov subspace that involves working directly with the Floquet unitary  $U$ , rather than with the Floquet Hamiltonian  $H_F$ . We discuss this alternate approach in the next section.

#### IV. KRYLOV CHAIN FROM THE ARNOLDI ITERATION

We now discuss a different Krylov subspace, one that arises from the action of  $U$  on the seed operator and is known as the Arnoldi iteration [31]. This differs from the previous section where the generator of the dynamics was a Hermitian operator, the Floquet Hamiltonian  $TH_F = i \ln U$ . Instead, we now work with a unitary operator, and below we outline the steps for obtaining the corresponding Krylov subspace.

Instead of  $\mathcal{L}$ , we now have the quantity  $W$  which is defined as follows

$$W|O\rangle = U^\dagger \hat{O} U \quad (21)$$

$$W^n|O\rangle = [U^\dagger]^n \hat{O} [U]^n. \quad (22)$$

$W$  is unitary because

$$W^\dagger W|O\rangle = U(U^\dagger \hat{O} U)U^\dagger \quad (23)$$

$$= \hat{O} = WW^\dagger|O\rangle. \quad (24)$$

We now outline the Arnoldi method. This reduces to the Lanczos scheme outlined in the previous section when  $W$  is Hermitian. In particular we will see that the unitarity of  $W$  will no longer produce a simple tri-diagonal matrix. Hermiticity is needed for the appearance of a tri-diagonal form as we saw in the previous section on the Lanczos iteration scheme.

Let  $|1\rangle = \sigma_1^x$ , then assuming we have found the orthonormal basis vectors  $|n\rangle, |n-1\rangle, \dots$ , we find  $|n+1\rangle$  by time evolving it, and projecting out the overlaps with the known basis vectors. Thus we have

$$\begin{aligned} |n+1'\rangle &= W|n\rangle - \sum_{l=1}^n |l\rangle \langle l|W|n\rangle \\ &= W|n\rangle - \sum_{l=1}^n w_{l,n}|l\rangle \end{aligned} \quad (25)$$

$$= \left[ 1 - \sum_{l=1}^n |l\rangle \langle l| \right] W|n\rangle = P_n W|n\rangle. \quad (26)$$

Above  $w_{l,n} = \langle l|W|n\rangle$  and  $P_n = 1 - \sum_{l=1}^n |l\rangle \langle l|$  projects out overlaps with the previously calculated basis vectors. Following this we normalize  $|n+1'\rangle$ ,

$$|n+1\rangle = \frac{|n+1'\rangle}{\sqrt{\langle n+1'|n+1'\rangle}}. \quad (27)$$

We note that

$$(n+1'|n+1') = (n+1'|P_n W|n\rangle) = (n+1'|W|n\rangle), \quad (28)$$

because  $(n+1'|l\rangle) = 0$  for  $l = 1 \dots n$  due to the projector  $P_n$ . Using Eq. (27) the above becomes

$$(n+1'|n+1') = \sqrt{\langle n+1'|n+1'\rangle} (n+1|W|n\rangle), \quad (29)$$

implying that

$$\sqrt{\langle n+1'|n+1'\rangle} = (n+1|W|n\rangle) = w_{n+1,n}. \quad (30)$$

Thus we start with  $|1\rangle$ , find  $W|1\rangle$  and  $\langle 1|W|1\rangle = w_{1,1}$ . Following this we find the unnormalized  $|2'\rangle = W|1\rangle - w_{1,1}|1\rangle$ . Then we determine the coefficient  $w_{2,1}$  from  $\langle 2'|2'\rangle = w_{2,1}^2$ . This first step fills in the first two rows of the first column of  $W$  in the Arnoldi basis.

Flipping Eq. (25) around, we have

$$W|n\rangle = w_{n+1,n}|n+1\rangle + \sum_{l=1}^n w_{l,n}|l\rangle. \quad (31)$$

Thus as we iterate through this Arnoldi algorithm, we will find that  $W$  has the following upper Hessenberg form

$$W = \begin{pmatrix} w_{1,1} & w_{1,2} & \dots \\ w_{2,1} & w_{2,2} & \dots \\ 0 & w_{3,2} & \dots \\ \vdots & \vdots & \ddots \end{pmatrix}. \quad (32)$$

An upper Hessenberg matrix is a square matrix whose elements  $w_{i,j} = 0$  for  $i > j + 1$ , i.e, it is a matrix whose elements are zero below the first sub-diagonal [41]. In addition, when the seed operator is Hermitian, all the elements of  $W$  are real because under time-evolution a Hermitian operator stays Hermitian, with the matrix elements of  $W$  simply denoting the weight of different Hermitian operators at a particular step in the iterative procedure. Typically the structure of  $W$  is such that the elements on the first sub-diagonal are dominant. These elements besides measuring the norm of the operators (see Eq. (30)), also measure how much the operator is spreading into new parts of the Krylov subspace. In contrast, all other elements of  $W$  are simply the overlap of the new operator generated at each iteration, with previous elements of the Krylov subspace. Moreover, the further an element is from the first sub-diagonal, the smaller it is. This observation will be handy later when we derive analytic expressions for  $W$ .

The autocorrelation function in terms of  $W$  now has the form

$$A_\infty(nT) = \langle 1|W^n|1\rangle. \quad (33)$$

Just as for  $\mathcal{L}$ , the iteration must be cut short after  $N$  steps. Due to the truncation, the resulting  $W$  will not be unitary. As we will show later in the context of ASZMs and ASPMs, as long as  $N$  is sufficiently large, the truncated  $W$  does well in reproducing the dynamics. The

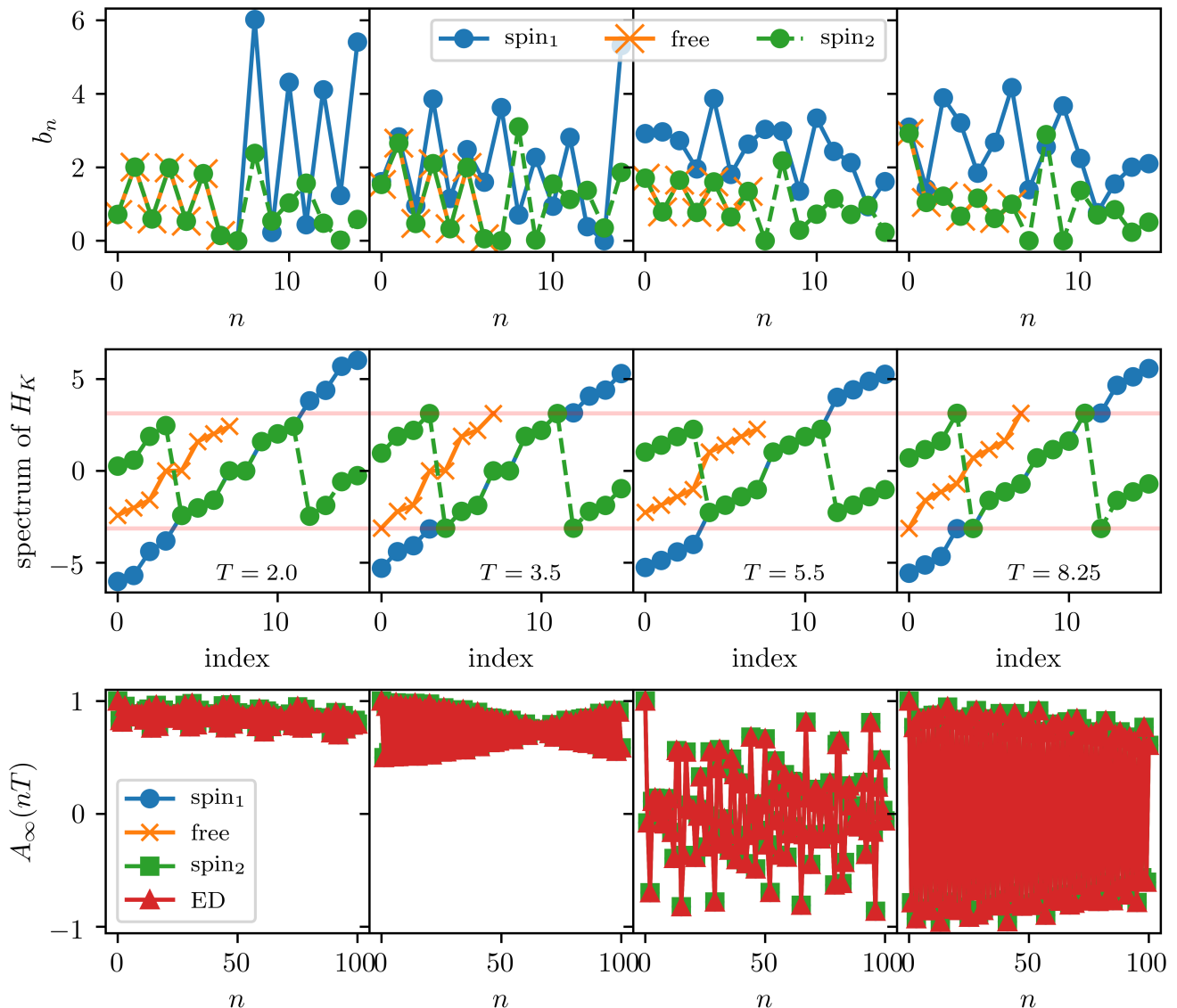


FIG. 4. Exploring the difference between the spin basis and the Majorana basis for the binary drive with  $g = 0.3$  and  $L = 4$ . All rows, from left to right  $T = 2.0, 3.5, 5.5, 8.25$ . These correspond respectively to SZM, SZM-SPM, trivial, and SPM phases. Top rows show the  $b_n$ s for the Majorana basis (labeled as “free”), and the two spin bases (labeled as  $\text{spin}_{1,2}$ ), where  $\text{spin}_1$  is the basis that gives the unfolded spectrum, while  $\text{spin}_2$  is the basis that gives the spectrum folded into the FBZ. Middle rows show the spectra of the corresponding Krylov Hamiltonians, with the  $x$ -axis label “index” labeling the eigenvalues. The bottom rows plot  $A_\infty$  obtained from performing the time-evolution using the three different Krylov Hamiltonians. The red data labeled as “ED” in the bottom rows is  $A_\infty$  from ED.

success of the approximation is a good indication that if the edge modes are sufficiently localized at the edge of the Krylov chain, the truncation scheme does not affect the physics.

We note that for the last state  $|N\rangle$  we have,

$$W|N\rangle = \sum_{l=1}^N w_{l,N}|l\rangle + w_{N+1,N}|N+1\rangle, \quad (34)$$

and by stopping at  $|N\rangle$ , we are making some form of a Markov approximation at a rate of  $w_{N+1,N}$ . Thus we

expect almost all operator dynamics produced by a truncated  $W$  to eventually cause a decay in time.

### A. Strong modes in limiting cases

We now discuss the form of the  $W$  matrix for some analytically tractable limiting cases. These limits were already discussed in previous sections in the context of the matrix  $K$  in Eq. (9).

- $Tg = (2n + 1)\pi$ ,  $T$  arbitrary: For this case  $e^{-iTgH_z/2} \propto \mathcal{D}$ , thus  $U^\dagger \sigma_1^x U = \mathcal{D} \sigma_1^x \mathcal{D} = -\sigma_1^x$ , and a SPM exists, whereas there is no SZM. The first step of the Arnoldi iteration is  $|1\rangle = \sigma_1^x$  and the next state is

$$|2'\rangle = W|1\rangle = -|1\rangle. \quad (35)$$

Thus the Krylov subspace terminates after the first basis vector  $|1\rangle = \sigma_1^x$ , and  $W$  is a "matrix" with a single element,  $-1$ .

- $Tg = (2n)\pi$ ,  $T$  arbitrary: For this case  $e^{-iTgH_z/2} \propto 1$  and  $U^\dagger \sigma_1^x U = \sigma_1^x$ . We have a SZM, but no SPM. Following the same steps as in the previous case, it is clear that  $W = 1$ .
- $T = (2n + 1)\pi$ ,  $Tg$  arbitrary: We now have  $e^{-iTgH_z/2} \propto \sigma_1^x \sigma_L^x$ , with  $e^{-iTgH_z/2} = \prod_l [\cos(Tg/2) - i\sigma_l^z \sin(Tg/2)]$ . For this case Eq. (11) holds. We now construct the Krylov subspace for  $\sigma_1^x$ . Beginning with  $|1\rangle = \sigma_1^x$ , we have using Eq. (11)

$$W|1\rangle = \cos(Tg)\sigma_1^x - \sin(Tg)\sigma_1^y, \quad (36)$$

giving,

$$|2'\rangle = W|1\rangle - \cos(Tg)|1\rangle = -\sin(Tg)\sigma_1^y. \quad (37)$$

After normalization we obtain

$$|2\rangle = -\sigma_1^y. \quad (38)$$

Moreover, again using Eq. (11), we can see that  $W|2\rangle$  will be a linear combination of  $|1\rangle, |2\rangle$ , and in particular

$$W = \begin{pmatrix} \cos(Tg) & |\sin(Tg)| \\ |\sin(Tg)| & -\cos(Tg) \end{pmatrix}, \quad (39)$$

which corresponds to having both a SZM and a SPM because the eigenvalues of  $W$  are  $\pm 1$ .

- $T = 2n\pi$  and  $Tg$  arbitrary: For this case we have  $e^{-iTJ_x H_{xx}/2} \propto 1$  and the time-evolution is given by Eq. (12). Carrying out the same steps as before one finds that the Krylov subspace for  $\sigma_1^x$  is two dimensional with

$$W = \begin{pmatrix} \cos(Tg) & -|\sin(Tg)| \\ |\sin(Tg)| & \cos(Tg) \end{pmatrix}. \quad (40)$$

Thus the eigenvalues are pure phases that do not equal  $\pm 1$ , unless  $Tg = n\pi$ , where  $n$  is an integer. When  $n \in \text{even}$ , we have a SZM, and when  $n \in \text{odd}$ , we have a SPM.

## V. ARNOLDI ITERATION FOR THE BINARY DRIVE

In this section we present the analytic form of  $W$  for the binary drive, and discuss it for some limiting cases which are more general than those discussed in the previous section. This discussion is aimed at showing the connection between strong modes and the topological properties of the Hamiltonian  $i \ln W$ .

Recall that for the binary drive, we can work in the Majorana basis where a chain of length  $L$  requires diagonalizing the problem in a reduced Hilbert space of size  $2L$ . It is straightforward, but tedious to verify that for a chain of length  $L = 4$  the Arnoldi algorithm produces the following  $8 \times 8$   $W$  matrix,

$$W = \begin{pmatrix} c_1 & -s_1 c_2 & s_2 s_1 c_1 & -s_2 s_1^2 c_2 & s_2^2 s_1^2 c_1 & -s_2^2 s_1^3 c_2 & s_2^3 s_1^3 c_1 & -s_2^3 s_1^4 \\ s_1 & c_2 c_1 & -s_2 c_1^2 & s_1 c_1 s_2 c_2 & -s_2^2 s_1 c_1^2 & s_2^2 s_1^2 c_2 c_1 & -s_2^3 s_1^2 c_1^2 & s_2^3 s_1^3 c_1 \\ 0 & s_2 & c_2 c_1 & -s_1 c_2^2 & s_1 c_1 s_2 c_2 & -s_2 s_1^2 c_2^2 & s_2^2 s_1^2 c_2 c_1 & -s_2^3 s_1^3 c_2 \\ 0 & 0 & s_1 & c_2 c_1 & -s_2 c_1^2 & s_1 c_1 s_2 c_2 & -s_2^2 s_1 c_1^2 & s_2^2 s_1^2 c_1 \\ 0 & 0 & 0 & s_2 & c_2 c_1 & -s_1 c_2^2 & s_1 c_1 s_2 c_2 & -s_2 s_1^2 c_2 \\ 0 & 0 & 0 & 0 & s_1 & c_2 c_1 & -s_2 c_1^2 & s_1 c_1 s_2 \\ 0 & 0 & 0 & 0 & 0 & s_2 & c_2 c_1 & -s_1 c_2 \\ 0 & 0 & 0 & 0 & 0 & 0 & s_1 & c_1 \end{pmatrix}, \quad (41)$$

where  $c_{1,2}, s_{1,2}$  were defined in Eq. (8). We discuss the structure of  $W$  as it will help us make further approximations. Firstly since  $W$  is unitary, its rows and columns form an orthonormal basis. Secondly, for even rows, starting on the column corresponding to the sub-diagonal, we have

$$\{s_1, c_1 c_2, -s_2 c_1^2, (s_1 s_2) c_1 c_2, -(s_1 s_2) s_2 c_1^2, \dots, (s_1 s_2)^n (c_1 c_2), (s_1 s_2)^n (-s_2 c_1^2), \dots\}. \quad (42)$$

Thirdly, for odd rows, starting on the column corresponding to the sub-diagonal, we have

$$\{s_2, c_1 c_2, -s_1 c_2^2, (s_1 s_2) c_1 c_2, -(s_1 s_2) s_1 c_2^2, \dots, (s_1 s_2)^n (c_1 c_2), (s_1 s_2)^n (-s_1 c_2^2), \dots\}. \quad (43)$$

The rows and columns at the edge of the matrix can be determined from using the above rules and then dividing by  $c_2$ . This also ensures orthonormality of the rows and columns. In what follows we will further explore  $W$ , and in particular  $\ln W$  for limiting cases that give SZMs and SPMs. The reason for exploring  $\ln W$  is that it has a Hamiltonian description, and therefore the topological properties can be more easily discerned.

### A. $\ln W$ for $gT \ll 1$ , $T \ll 1$ : SZM phase

First let us consider the case when  $gT \ll 1$ . For this case we have  $s_2, c_2$  arbitrary, and  $s_1 \ll 1, c_1 \approx 1$ . Truncating the  $W$  matrix in Eq. (41) to terms of  $O(s_1)$  we have

$$W = \begin{pmatrix} 1 & -s_1 c_2 & s_2 s_1 & 0 & 0 & 0 & 0 & 0 \\ s_1 & c_2 & -s_2 & s_1 s_2 c_2 & -s_2^2 s_1 & 0 & 0 & 0 \\ 0 & s_2 & c_2 & -s_1 c_2^2 & s_1 s_2 c_2 & 0 & 0 & 0 \\ 0 & 0 & s_1 & c_2 & -s_2 & s_1 s_2 c_2 & -s_2^2 s_1 & 0 \\ 0 & 0 & 0 & s_2 & c_2 & -s_1 c_2^2 & s_1 s_2 c_2 & 0 \\ 0 & 0 & 0 & 0 & s_1 & c_2 & -s_2 & s_1 s_2 \\ 0 & 0 & 0 & 0 & 0 & s_2 & c_2 & -s_1 c_2 \\ 0 & 0 & 0 & 0 & 0 & 0 & s_1 & 1 \end{pmatrix} + O(s_1^2) = W_0 + \delta W, \quad (44)$$

$$W_0 = \begin{pmatrix} 1 & 0 & 0 & 0 & 0 & 0 & 0 & 0 \\ 0 & c_2 & -s_2 & 0 & 0 & 0 & 0 & 0 \\ 0 & s_2 & c_2 & 0 & 0 & 0 & 0 & 0 \\ 0 & 0 & 0 & c_2 & -s_2 & 0 & 0 & 0 \\ 0 & 0 & 0 & s_2 & c_2 & 0 & 0 & 0 \\ 0 & 0 & 0 & 0 & 0 & c_2 & -s_2 & 0 \\ 0 & 0 & 0 & 0 & 0 & s_2 & c_2 & 0 \\ 0 & 0 & 0 & 0 & 0 & 0 & 0 & 1 \end{pmatrix} = W(gT = 0), \quad (45)$$

$$\delta W = \begin{pmatrix} 0 & -s_1 c_2 & s_2 s_1 & 0 & 0 & 0 & 0 & 0 \\ s_1 & 0 & 0 & s_1 s_2 c_2 & -s_2^2 s_1 & 0 & 0 & 0 \\ 0 & 0 & 0 & -s_1 c_2^2 & s_1 s_2 c_2 & 0 & 0 & 0 \\ 0 & 0 & s_1 & 0 & 0 & s_1 s_2 c_2 & -s_2^2 s_1 & 0 \\ 0 & 0 & 0 & 0 & 0 & -s_1 c_2^2 & s_1 s_2 c_2 & 0 \\ 0 & 0 & 0 & 0 & s_1 & 0 & 0 & s_1 s_2 \\ 0 & 0 & 0 & 0 & 0 & 0 & 0 & -s_1 c_2 \\ 0 & 0 & 0 & 0 & 0 & 0 & s_1 & 0 \end{pmatrix}. \quad (46)$$

Above  $W_0 = W(gT = 0)$ , while  $\delta W$  is the leading correction about this point and is  $O(s_1)$ . If in addition we impose  $T \ll 1$  which is equivalent to  $s_2 \ll 1$ , the matrices  $W_0$  and  $\delta W$  commute if terms of  $O(s_1 s_2), O(s_1^2), O(s_2^2)$  and higher are dropped. Recall that if  $A$  and  $B$  are two commuting matrices  $[A, B] = 0$ , then,

$$\ln(A + B) \approx \ln[A] + [A]^{-1} B + \dots \quad (47)$$

Using, Eq. (47) and setting  $A = W_0, B = \delta W$ , we find the following expressing to first order in  $s_1$  and  $T$

$$i \ln[W] \approx \begin{pmatrix} 0 & -is_1 & 0 & 0 & 0 & 0 & 0 & 0 \\ is_1 & 0 & -iT & 0 & 0 & 0 & 0 & 0 \\ 0 & iT & 0 & -is_1 & 0 & 0 & 0 & 0 \\ 0 & 0 & is_1 & 0 & -iT & 0 & 0 & 0 \\ 0 & 0 & 0 & iT & 0 & -is_1 & 0 & 0 \\ 0 & 0 & 0 & 0 & is_1 & 0 & -iT & 0 \\ 0 & 0 & 0 & 0 & 0 & iT & 0 & -is_1 \\ 0 & 0 & 0 & 0 & 0 & 0 & is_1 & 0 \end{pmatrix}. \quad (48)$$

Above  $i \ln W$  represents a Floquet Hamiltonian that is effectively a SSH model with topologically non-trivial sign of the dimerization for  $|s_1| < T$ . Thus a zero mode is guaranteed. This shows that the SZM of the original Hamiltonian manifests as an edge mode of a topologically non-trivial Hamiltonian  $i \ln W$  in the single particle Krylov subspace.

### B. $\ln W$ for $gT \approx \pi$ , $T \ll 1$ : SPM phase

Let us first consider  $gT \approx \pi$  where  $s_1 \ll 1$  and  $c_1 = -1$ . Truncating  $W$  in Eq. (41) to  $O(s_1)$  we obtain

$$W = \begin{pmatrix} -1 & -s_1 c_2 & -s_2 s_1 & 0 & 0 & 0 & 0 & 0 \\ s_1 & -c_2 & -s_2 & -s_1 s_2 c_2 & -s_2^2 s_1 & 0 & 0 & 0 \\ 0 & s_2 & -c_2 & -s_1 c_2^2 & -s_1 s_2 c_2 & 0 & 0 & 0 \\ 0 & 0 & s_1 & -c_2 & -s_2 & -s_1 s_2 c_2 & -s_2^2 s_1 & 0 \\ 0 & 0 & 0 & s_2 & -c_2 & -s_1 c_2^2 & -s_1 s_2 c_2 & 0 \\ 0 & 0 & 0 & 0 & s_1 & -c_2 & -s_2 & -s_1 s_2 \\ 0 & 0 & 0 & 0 & 0 & s_2 & -c_2 & -s_1 c_2 \\ 0 & 0 & 0 & 0 & 0 & 0 & s_1 & -1 \end{pmatrix} + O(s_1^2) = W_0 + \delta W, \quad (49)$$

$$W_0 = W(gT = \pi) = - \begin{pmatrix} 1 & 0 & 0 & 0 & 0 & 0 & 0 & 0 \\ 0 & c_2 & s_2 & 0 & 0 & 0 & 0 & 0 \\ 0 & -s_2 & c_2 & 0 & 0 & 0 & 0 & 0 \\ 0 & 0 & 0 & c_2 & s_2 & 0 & 0 & 0 \\ 0 & 0 & 0 & -s_2 & c_2 & 0 & 0 & 0 \\ 0 & 0 & 0 & 0 & 0 & c_2 & s_2 & 0 \\ 0 & 0 & 0 & 0 & 0 & -s_2 & c_2 & 0 \\ 0 & 0 & 0 & 0 & 0 & 0 & 0 & 1 \end{pmatrix}, \quad (50)$$

$$\delta W = \begin{pmatrix} 0 & -s_1 c_2 & -s_2 s_1 & 0 & 0 & 0 & 0 & 0 \\ s_1 & 0 & 0 & -s_1 s_2 c_2 & -s_2^2 s_1 & 0 & 0 & 0 \\ 0 & 0 & 0 & -s_1 c_2^2 & -s_1 s_2 c_2 & 0 & 0 & 0 \\ 0 & 0 & s_1 & 0 & 0 & -s_1 s_2 c_2 & -s_2^2 s_1 & 0 \\ 0 & 0 & 0 & 0 & 0 & -s_1 c_2^2 & -s_1 s_2 c_2 & 0 \\ 0 & 0 & 0 & 0 & s_1 & 0 & 0 & -s_1 s_2 \\ 0 & 0 & 0 & 0 & 0 & 0 & 0 & -s_1 c_2 \\ 0 & 0 & 0 & 0 & 0 & 0 & s_1 & 0 \end{pmatrix}.$$

Above  $\delta W$  is  $O(s_1)$ , and represents the leading correction to  $W$  around the point  $gT = \pi$ . If we now also assume  $T \ll 1$  which is equivalent to  $s_2 \ll 1$ , then  $W_0$  and  $\delta W$  commute if terms of  $O(s_1 s_2), O(s_1^2), O(s_2^2)$  and higher are dropped. Performing the expansion in Eq. (47) we find, to first order in  $s_1$  and  $T$

$$i \ln [W] \approx \pm \pi + \begin{pmatrix} 0 & i s_1 & 0 & 0 & 0 & 0 & 0 & 0 \\ -i s_1 & 0 & iT & 0 & 0 & 0 & 0 & 0 \\ 0 & -iT & 0 & i s_1 & 0 & 0 & 0 & 0 \\ 0 & 0 & -i s_1 & 0 & iT & 0 & 0 & 0 \\ 0 & 0 & 0 & -iT & 0 & i s_1 & 0 & 0 \\ 0 & 0 & 0 & 0 & -i s_1 & 0 & iT & 0 \\ 0 & 0 & 0 & 0 & 0 & -iT & 0 & i s_1 \\ 0 & 0 & 0 & 0 & 0 & 0 & -i s_1 & 0 \end{pmatrix}. \quad (51)$$

Thus we find that the Floquet Hamiltonian  $i \ln W$  now represents a topologically non-trivial SSH model (for  $|s_1| < T$ ), with a constant shift of  $\pi$ , the latter ensuring that the zero mode of the SSH model is shifted in energy by  $\pi$ . A similar picture was discussed in Ref. 30, where the discussion was presented for the Floquet Hamiltonian  $i \ln K$ .

### C. $\ln W$ for $T \approx \pi$ : SZM-SPM phase

Let us consider the case  $T \approx \pi$ . For this case we have  $c_2 \approx -1, s_2 \ll 1$  while  $c_1, s_1$  are arbitrary. Truncating Eq. (41) to  $O(s_2)$  we obtain

$$\begin{aligned}
W &= \begin{pmatrix} c_1 & s_1 & s_1 s_2 c_1 & s_1^2 s_2 & 0 & 0 & 0 & 0 \\ s_1 & -c_1 & -s_2 c_1^2 & -s_1 s_2 c_1 & 0 & 0 & 0 & 0 \\ 0 & s_2 & -c_1 & -s_1 & -s_1 s_2 c_1 & -s_1^2 s_2 & 0 & 0 \\ 0 & 0 & s_1 & -c_1 & -s_2 c_1^2 & -s_1 s_2 c_1 & 0 & 0 \\ 0 & 0 & 0 & s_2 & -c_1 & -s_1 & -s_1 s_2 c_1 & s_1^2 s_2 \\ 0 & 0 & 0 & 0 & s_1 & -c_1 & -s_2 c_1^2 & s_1 s_2 c_1 \\ 0 & 0 & 0 & 0 & 0 & s_2 & -c_1 & s_1 \\ 0 & 0 & 0 & 0 & 0 & 0 & s_1 & c_1 \end{pmatrix} + O(s_2^2) = W_0 + \delta W, \quad (52) \\
W_0 = W(T = \pi) &= \begin{pmatrix} c_1 & s_1 & 0 & 0 & 0 & 0 & 0 & 0 \\ s_1 & -c_1 & 0 & 0 & 0 & 0 & 0 & 0 \\ 0 & 0 & -c_1 & -s_1 & 0 & 0 & 0 & 0 \\ 0 & 0 & s_1 & -c_1 & 0 & 0 & 0 & 0 \\ 0 & 0 & 0 & 0 & -c_1 & -s_1 & 0 & 0 \\ 0 & 0 & 0 & 0 & s_1 & -c_1 & 0 & 0 \\ 0 & 0 & 0 & 0 & 0 & 0 & -c_1 & s_1 \\ 0 & 0 & 0 & 0 & 0 & 0 & s_1 & c_1 \end{pmatrix} \\
&= \begin{pmatrix} \pm i e^{\mp i \frac{\pi}{2} (c_1 \sigma_z + s_1 \sigma_x)} & 0 & 0 & 0 & 0 & 0 & 0 & 0 \\ 0 & 0 & 0 & 0 & 0 & 0 & 0 & 0 \\ 0 & 0 & -e^{iT \sigma_y} & 0 & 0 & 0 & 0 & 0 \\ 0 & 0 & 0 & 0 & 0 & 0 & 0 & 0 \\ 0 & 0 & 0 & 0 & -e^{iT \sigma_y} & 0 & 0 & 0 \\ 0 & 0 & 0 & 0 & 0 & 0 & 0 & 0 \\ 0 & 0 & 0 & 0 & 0 & 0 & 0 & \pm i e^{\mp i \frac{\pi}{2} (-c_1 \sigma_z + s_1 \sigma_x)} \end{pmatrix}, \\
\delta W &= \begin{pmatrix} 0 & 0 & s_1 s_2 c_1 & s_1^2 s_2 & 0 & 0 & 0 & 0 \\ 0 & 0 & -s_2 c_1^2 & -s_1 s_2 c_1 & 0 & 0 & 0 & 0 \\ 0 & s_2 & 0 & 0 & -s_1 s_2 c_1 & -s_1^2 s_2 & 0 & 0 \\ 0 & 0 & 0 & 0 & -s_2 c_1^2 & -s_1 s_2 c_1 & 0 & 0 \\ 0 & 0 & 0 & s_2 & 0 & 0 & -s_1 s_2 c_1 & s_1^2 s_2 \\ 0 & 0 & 0 & 0 & 0 & 0 & -s_2 c_1^2 & s_1 s_2 c_1 \\ 0 & 0 & 0 & 0 & 0 & s_2 & 0 & 0 \\ 0 & 0 & 0 & 0 & 0 & 0 & 0 & 0 \end{pmatrix}. \quad (53)
\end{aligned}$$

Above  $\delta W$  is the leading correction to  $W_0$  and is  $O(s_2)$ .

At this stage we simply discuss the Floquet Hamiltonian  $i \ln(W_0)$ ,

$$\ln[W_0] \approx \begin{pmatrix} 0 & 0 & 0 & 0 & 0 & 0 & 0 & 0 \\ \ln \left[ \pm i e^{\mp i \frac{\pi}{2} (c_1 \sigma_z + s_1 \sigma_x)} \right] & 0 & 0 & 0 & 0 & 0 & 0 & 0 \\ 0 & 0 & 0 & 0 & 0 & 0 & 0 & 0 \\ 0 & 0 & \ln \left[ -e^{iT \sigma_y} \right] & 0 & 0 & 0 & 0 & 0 \\ 0 & 0 & 0 & 0 & 0 & 0 & 0 & 0 \\ 0 & 0 & 0 & 0 & \ln \left[ -e^{iT \sigma_y} \right] & 0 & 0 & 0 \\ 0 & 0 & 0 & 0 & 0 & 0 & 0 & 0 \\ 0 & 0 & 0 & 0 & 0 & 0 & 0 & \ln \left[ \pm i e^{\mp i \frac{\pi}{2} (-c_1 \sigma_z + s_1 \sigma_x)} \right] \end{pmatrix}. \quad (54)$$

Thus we see that  $i \ln(W_0)$ , for these parameters, has a complex edge structure represented by the  $2 \times 2$  block in the upper and lower diagonals. The eigenvalues of these edge modes are  $0, \pm \pi$ . Moreover, these edge modes are completely decoupled from a bulk which has a dimerization of a topologically non-trivial SSH model represented by

the repeated sub-block  $\ln \left[ -e^{iT\sigma_y} \right]$ . Deviating from this exactly solvable limit will couple the edge modes weakly to the bulk states, and will also generate longer range hopping. However, these edge modes are protected as long as the bulk gap remains non-zero. Thus we see that the SZM-SPM phase also can be interpreted as topologically protected edge modes of a single-particle Hamiltonian in Krylov subspace. The advantage of the discussion in this section is that, even when interactions are non-zero, one may construct an effectively single-particle  $W$ . Thus, topological features, or lack thereof, of  $W$  can shed light on the lifetime of the almost strong modes.

## VI. LIFETIME OF EDGE MODES FROM THE ARNOLDI ALGORITHM

In this section we construct the approximate edge mode and derive its lifetime for the most general  $W$  matrix whose upper Hessenberg form is highlighted in Eq. (32). The results derived here hold for the free and the interacting cases. Recall that for the free system we have a SZM and/or a SPM. These acquire a lifetime due to finite size effects, i.e, their lifetime scales exponentially in the system size  $L$ . On the other hand, when the interactions are non-zero, the edge modes acquire a system-size independent lifetime provided the system size is large enough. For small system sizes, there is not much of a difference between strong modes and almost strong modes as both have lifetimes that grow exponentially with system size.

We denote edge modes of  $W$ , both exact and approximate, as  $|\psi_{0,\pi}\rangle$ , where the subscript indicates whether it is a zero mode or a  $\pi$ -mode. We then argue that the lifetime  $\gamma_{0,\pi}^{-1}$  of the edge mode is well approximated by the expression

$$e^{-\gamma_{0,\pi}} = |\langle \psi_{0,\pi} | W | \psi_{0,\pi} \rangle|, \quad (55)$$

where  $\gamma_{0,\pi}$  is in dimensionless units. We will present numerical evidence for this. It is straightforward to see that when  $|\psi_{0,\pi}\rangle$  are exact edge modes,  $|\langle \psi_{0,\pi} | W | \psi_{0,\pi} \rangle| = 1$  and the decay rate  $\gamma_{0,\pi} = 0$ . We will apply the formula to the case where we have quasi-stable edge modes, so that  $|\langle \psi_{0,\pi} | W | \psi_{0,\pi} \rangle| < 1$ , resulting in a non-zero decay rate.

We solve for the edge modes by determining the left eigenvectors of  $W$ ,

$$\langle \psi_{0,\pi} | W = \tilde{\lambda} \langle \psi_{0,\pi} |, \quad (56)$$

with  $\tilde{\lambda} = 1$  for  $\langle \psi_0 |$  and  $\tilde{\lambda} = -1$  for  $\langle \psi_\pi |$ . Essentially this allows us to work from the first site and iterate into the bulk. We denote the elements of  $\langle \psi_{0,\pi} |$  by  $\psi_i$  where the subscript  $i$  is the site index. The first step involves the inner product of the left eigenvector with the first column of  $W - \tilde{\lambda}$  which gives

$$\psi_1 = 1, \quad (57)$$

$$\psi_2 = -\left( \frac{w_{1,1} - \tilde{\lambda}}{w_{2,1}} \right). \quad (58)$$

Above we set  $\psi_1 = 1$  as we are interested in an edge mode. The inner product of the left eigenvector onto the second column of the matrix  $W - \tilde{\lambda}$  gives

$$\psi_3 = -\frac{1}{w_{3,2}} \left[ (w_{2,2} - \tilde{\lambda})\psi_2 + w_{1,2}\psi_1 \right]. \quad (59)$$

The pattern is clear for the rest of the eigenvector components,

$$\psi_{n+1} = -\frac{1}{w_{n+1,n}} \left[ (w_{n,n} - \tilde{\lambda})\psi_n + \sum_{i=1}^{n-1} w_{i,n}\psi_i \right], \quad (60)$$

with a final normalization step at the end of the calculation.

We now rewrite Eq. (60) as follows as it will be helpful later

$$\sum_{i=1}^{n-1} \psi_i w_{i,n} = -\psi_{n+1} w_{n+1,n} - (w_{n,n} - \tilde{\lambda})\psi_n. \quad (61)$$

Since all the elements of  $W$  are real, the components  $\psi_i$  of the edge mode are also real. We now set out to compute the right hand side of Eq. (55). It is straightforward to see that

$$\langle \psi_{0,\pi} | W | \psi_{0,\pi} \rangle = \sum_{k=1}^{N-1} \left[ \psi_{k+1} w_{k+1,k} + \psi_k w_{k,k} + \sum_{m=1}^{k-1} \psi_m w_{m,k} \right] \psi_k + \sum_{m=1}^N \psi_m w_{m,N} \psi_N \quad (62)$$

$$= \sum_{k=1}^{N-1} \left[ \psi_{k+1} w_{k+1,k} + \psi_k w_{k,k} + \left( -\psi_{k+1} w_{k+1,k} - (w_{k,k} - \tilde{\lambda}) \psi_k \right) \right] \psi_k + \sum_{m=1}^N \psi_m w_{m,N} \psi_N \quad (63)$$

$$= \sum_{k=1}^{N-1} \tilde{\lambda} \psi_k^2 + \sum_{m=1}^N \psi_m w_{m,N} \psi_N \quad (64)$$

$$= \tilde{\lambda} \left[ \sum_{k=1}^N \psi_k^2 + \tilde{\lambda} \sum_{m=1}^N \psi_m w_{m,N} \psi_N - \psi_N^2 \right]. \quad (65)$$

In the second equality above we have used Eq. (61) to simplify the expression.

We normalize  $\psi_{0,\pi} \rightarrow \psi_{0,\pi}/N_{0,\pi}$  and use that  $|\tilde{\lambda}| = 1$  to obtain

$$|\langle \psi_{0,\pi} | W | \psi_{0,\pi} \rangle| = 1 + \frac{\tilde{\lambda}}{N_{0,\pi}^2} \sum_{m=1}^N \psi_m w_{m,N} \psi_N - \frac{\psi_N^2}{N_{0,\pi}^2}. \quad (66)$$

Using Eq. (55), we identify the decay rate from Taylor expanding the left hand side of the same equation to obtain

$$\gamma_{0,\pi} \approx \frac{\psi_N^2}{N_{0,\pi}^2} - \frac{\tilde{\lambda}}{N_{0,\pi}^2} \sum_{m=1}^N \psi_m w_{m,N} \psi_N. \quad (67)$$

We cannot proceed further without making approximations to  $W$  or to  $\psi$ . As it stands, Eq. (67) agrees well with the quantity  $\ln |\langle \psi_{0,\pi} | W | \psi_{0,\pi} \rangle|$  which was how the decay-rate was defined in Eq. (55). We give evidence of this in the next section. Empirically, we also find that the second term in Eq. (67) is often much smaller than the first, thus we can approximate the expression for the decay rate even further as

$$\gamma_{0,\pi} \approx \psi_N^2. \quad (68)$$

Above we are explicitly working with the normalized wavefunction and therefore we have dropped the factor of  $N_{0,\pi}^2$ .

Thus the decay rate is the probability of the edge mode to be located at the site  $N$ . Recall that  $N$  is the dimension of the  $W$  matrix. For the free case, if  $N = 2L$ , this exhausts the Hilbert space. For the interacting problem  $N$  has to be very large  $\approx e^{2L}$  in order to exhaust the Hilbert space. Thus when working with interacting systems, we will always be truncating  $W$ . However as long as this truncation occurs for an  $N$  which is large enough, and the quasi-stable edge mode is sufficiently localized at the edge, the decay rate  $\gamma_{0,\pi}$ , and therefore the probability of finding the particle at site  $N$ , will be independent of  $N$  (for a given system size  $L$ ).

## VII. KRYLOV SUBSPACE WITH INTERACTIONS

We now consider the interacting example by modifying the binary drive in Eq. (1) into a ternary drive where the third part of the drive breaks the free fermion nature of the problem. Specifically we study

$$U = e^{-i\frac{T}{2} J_z H_{zz}} e^{-i\frac{T}{2} J_x H_{xx}} e^{-i\frac{T}{2} g H_z}, \quad (69)$$

where the interacting part is

$$H_{zz} = \sum_{i=1}^{L-1} \sigma_i^z \sigma_{i+1}^z. \quad (70)$$

The above drive was studied in detail in [22, 30], and it was found that the SZMs and SPMs get modified to ASZMs and ASPMs where the latter are characterized by a system size independent lifetime, for sufficiently large system sizes. Moreover, this lifetime is still very long as compared to the time needed for the bulk of the system to heat to infinite temperature. These studies were carried out employing the Lanczos iteration scheme. Therefore, we discuss the role of interactions only within the Arnoldi iteration scheme.

### A. Krylov subspace from the Arnoldi iteration

Section IV outlined the Arnoldi procedure. The key quantity is the unitary matrix  $W$  in Eq. (32) which has a characteristic upper Hessenberg form. The analytic expression for  $W$  and  $\ln W$  for the binary drive was presented in Section V, and the lifetime of the edge mode operators for the general case including interactions was derived in Section VI. In this section we present the  $W$  matrix for the interacting problem, and apply the results for the lifetime, derived in Section VI.

Fig. 5 shows the spectrum of  $i \ln W$  for the free case (top panel) and for the interacting case (bottom panel) where  $J_z = 0.05$  for the interacting case. All other parameters are common between the top and bottom panels. In particular,  $g = 0.3$ , the system size is  $L = 10$ , and

$W$  is a  $20 \times 20$  matrix. Thus for the free case,  $W$  is exact. However for the interacting case,  $W$  is not exact because the Hilbert space is larger than  $2L$ , and construction of the  $W$  matrix leads to truncation and loss of unitarity. A consequence of this is the appearance of unphysical zero modes. This is clearly seen in the lower left-most panel of Fig. 5 which shows three zero modes, while the upper panel (free case) shows only two zero modes. Thus the truncation for the interacting case has led to the appearance of an additional spurious zero mode.

To understand why spurious zero modes can appear on truncation, let us consider a  $W$  with a simple  $3 \times 3$  structure. The  $W$  have the property that the lower sub-diagonal (c.f. Eq. (30)) is the strongest as it measures the part of the operator that explores new regions of the Krylov subspace. For an ergodic system, it is natural that this element will be largest. However, an artificial truncation will cause a  $W$  of the form

$$W = \begin{pmatrix} 0 & 0 & 1 \\ 1 & 0 & 0 \\ 0 & 1 & 0 \end{pmatrix} \quad (71)$$

to become

$$W_{\text{trunc}} = \begin{pmatrix} 0 & 0 & 0 \\ 1 & 0 & 0 \\ 0 & 1 & 0 \end{pmatrix} \quad (72)$$

Now  $W_{\text{trunc}}$  has a null vector

$$W_{\text{trunc}} \begin{pmatrix} 0 \\ 0 \\ 1 \end{pmatrix} = 0 \quad (73)$$

This null vector is not shared by the untruncated  $W$ . Thus quite generally, the fact that the lower sub-diagonal is dominant in  $W$  can lead to the appearance of null vectors when the  $W$  matrix is truncated, where the null vectors have a large weight at the lower end.

We now discuss the (A)SPMs. The  $\pm\pi$  modes are clearly visible on the top panel, and they are found to persist in the presence of interactions, although the edge modes are not so well separated in energy from the bulk states when interactions are present. This is expected as we now have ASPMs which will now decay into the bulk. Sometimes the mode at  $-\pi$  can appear at  $\pi$  as seen in the lower fourth panel. This is not a spurious effect because  $-\pi$  and  $\pi$  states are degenerate states due to the periodicity of the spectrum. However the truncation can lead to spurious effects such as the disappearance of one of the  $\pi$  modes as can be seen in the lower second panel.

We now turn to the computation of  $A_\infty$  and extracting the lifetime. Fig. 6 shows the autocorrelation functions for  $g = 0.3$ ,  $J_z = 0.05$  and for the same set of  $T$  as Fig. 5. The top row is for  $L = 4$  while the bottom row is for  $L = 8$ . The blue dots are  $A_\infty$  from ED. The orange data are the  $A_\infty$  obtained from the  $W$  matrix, with the  $W$  matrix truncated to  $N = 18$ . We have checked that the

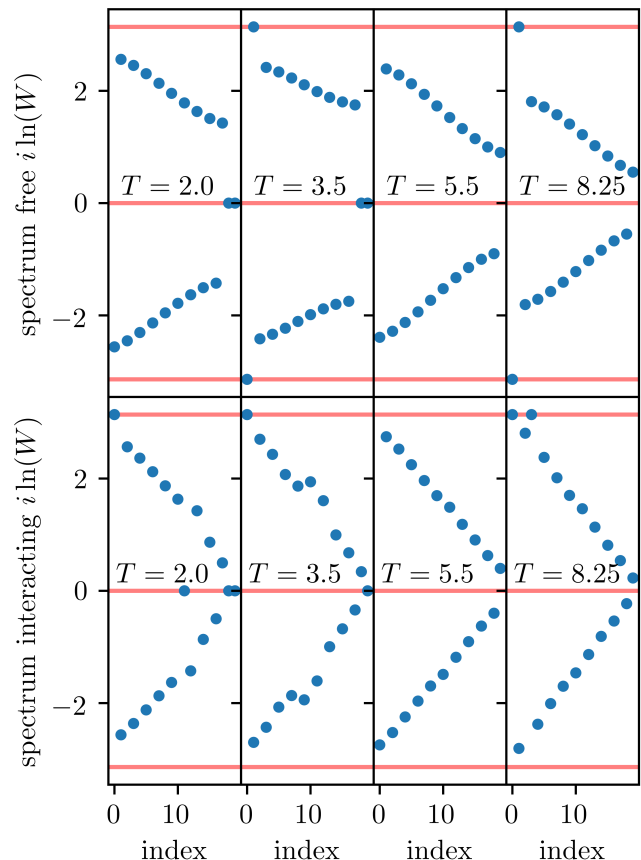


FIG. 5. Spectrum of  $i \ln W$  for free example (upper row) and an interacting example with  $J_z = 0.05$  (lower row).  $x$ -axis label “index” denotes the location of the eigenvalues arranged in descending order of their magnitude. For all data  $L = 10$  and  $W$  is a  $20 \times 20$  matrix. In addition  $g = 0.3$ . The four different values of  $T$  are from left to right  $T = 2.0, 3.5, 5.5, 8.25$ . These correspond respectively to (A)SZM, (A)SZM-(A)SPM, trivial, and (A)SPM phases. The horizontal red lines indicate  $0, \pm\pi$ .

truncation at  $N = 18$  does not influence the results for the system sizes chosen ( $L = 4, 8$ ).

The precise quantity being plotted in orange (labeled  $W$ ) is Eq. (33), but with some approximations made to it. In particular,

$$\begin{aligned} A_\infty(nT) &= \text{Tr} \left[ W^n |1\rangle\langle 1| \right] \\ &\approx \text{Tr} \left[ W^n \left( |\psi_0\rangle\langle\psi_0| + |\psi_\pi\rangle\langle\psi_\pi| \right) |1\rangle\langle 1| \right] \quad (74) \\ &= \sum_{\lambda=0,\pi} \psi_{\lambda,1} \langle 1| W^n |\psi_\lambda\rangle, \quad \psi_{\lambda,1} = \langle\psi_\lambda|1\rangle. \quad (75) \end{aligned}$$

Above  $|1\rangle$  is a state which is completely localized on the first site of the Krylov subspace. The approximation made in the second line involves replacing the complete set of states of  $W$  by only its edge modes  $|\psi_{\lambda=0,\pi}\rangle$ . Thus we are dropping all the bulk modes of  $W$ . Also note that,

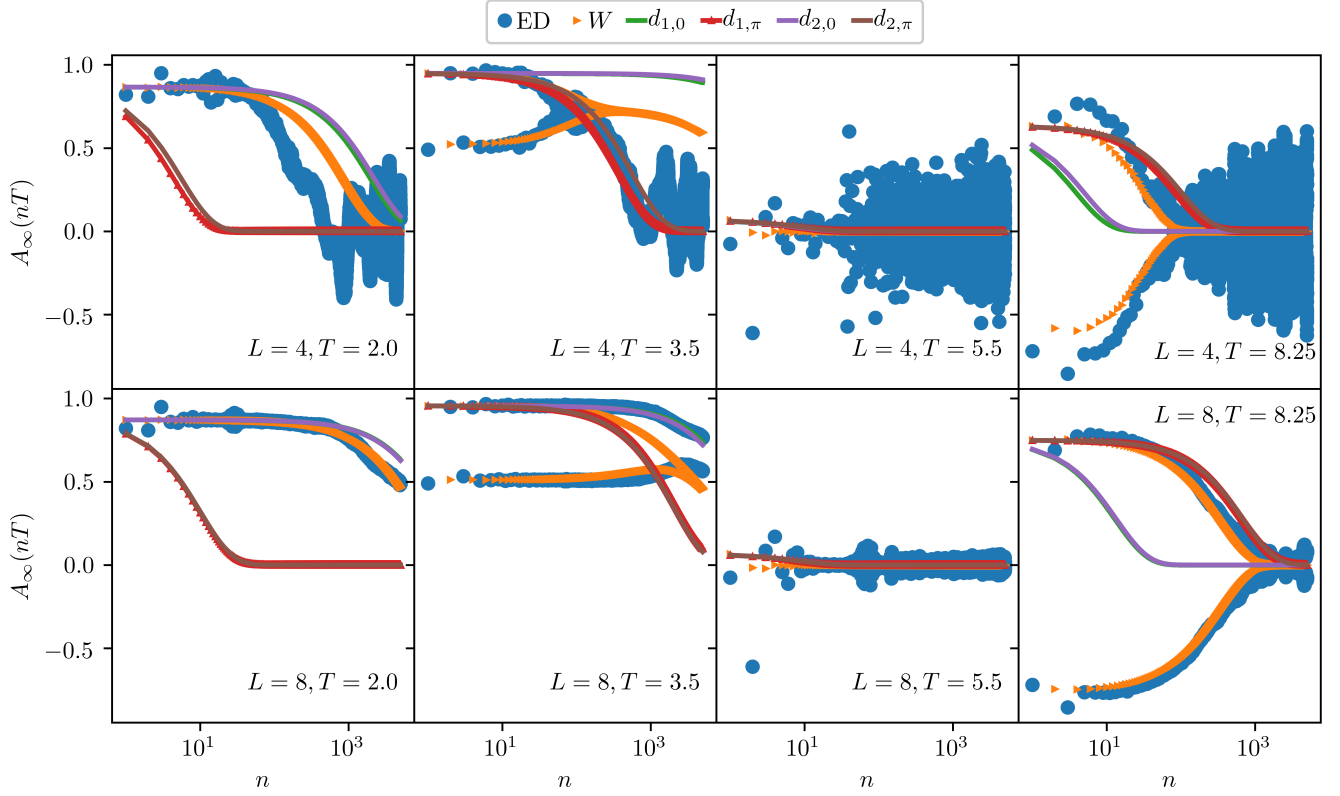


FIG. 6. Time evolution of approximate edge states of  $W$  (orange) for an interacting example ( $J_z = 0.05$ ) and compared to  $A_\infty$  obtained from ED (blue). The top row is for a very small system size of  $L = 4$  and the bottom row is for  $L = 8$ . The four columns compare four different phases. These are from left to right: ASZM phase ( $T = 2.0$ ), ASZM-ASPM phase ( $T = 3.5$ ), trivial phase ( $T = 5.5$ ), and ASPM phase ( $T = 8.25$ ).  $W$  is truncated to a  $18 \times 18$  matrix, and the time-evolution generated by it (orange) is according to Eq. (75). The data labeled by  $d_{1,\lambda}$ ,  $d_{2,\lambda}$  with  $\lambda = 0, \pi$  are two different approximations corresponding to Eq. (76) for  $d_{1,\lambda}$  and Eq. (77) for  $d_{2,\lambda}$ .

$\psi_{\lambda,1}$  is the normalized amplitude of the edge mode on the first site.

The results for  $A_\infty$  in Fig. 6 are compared to two different approximations. One is the data labeled as  $d_{1,\lambda=0,\pi}$  where

$$\begin{aligned} d_{1,\lambda}(nT) &= |\psi_{\lambda,1}|^2 e^{-\gamma_\lambda n} \\ &= |\psi_{\lambda,1}|^2 |\langle \psi_\lambda | W | \psi_\lambda \rangle|^n, \quad \lambda = 0, \pi. \end{aligned} \quad (76)$$

The above expression uses the definition of the decay-rate in Eq. (55) accounting for the amplitude  $\psi_{\lambda,1}$  of finding the particle on the first site, before the time-evolution. Since  $|\psi_{0,\pi}\rangle$  edge modes are only approximate edge modes, Eq. (76) does lead to a decay. The data set labeled by  $d_{2,\lambda=0,\pi}$  corresponds to approximating  $\gamma_{0,\pi}$  by Eq. (68), thus

$$d_{2,\lambda}(nT) = |\psi_{\lambda,1}|^2 e^{-|\psi_{\lambda,N}|^2 n}, \quad \lambda = 0, \pi, \quad (77)$$

where  $\psi_{\lambda,N}$  is the normalized amplitude of the  $\lambda = 0, \pi$  approximate edge mode at the last site  $N$ .

We find that  $W$ , despite its truncation, agrees very well with ED. In addition, the two approximations to  $W$  given

by Eq. (76) and Eq. (77) also agree well as far as capturing the decay rates are concerned. The approximations appear to not work quite so well for the second panel corresponding to the ASZM-ASPM phase ( $T = 3.5$ ). This may be because when both almost strong modes are present, as they decay they influence each other through the bulk states in a way that our simple approximation has not accounted for. However, the agreement does improve with increasing system size (compare upper and lower panels for  $T = 3.5$ ). In particular, when both ASZM and ASPM are present, the edge structure is more complex and has a  $2 \times 2$  structure at each end (see Section V). This can make the effective system size of  $L = 4$  (upper panels) look effectively shorter for an ASZM-ASPM phase as compared to an ASPM or an ASZM phase.

## VIII. CONCLUSIONS

Almost strong edge modes are quasi-stable edge modes that have unusually long lifetimes such that they can co-exist with a metallic bulk for many drive cycles. These edge modes include both zero modes as well as  $\pi$  modes,

where the latter show period doubled dynamics. It is notoriously hard to develop analytic methods for interacting and driven systems in general, and determining lifetimes of quasi-stable modes in particular. However in this paper, building on previous work [16, 17, 30], we showed a promising route which involves mapping the dynamics of the edge mode operator to single particle dynamics in Krylov subspace. While the detailed modeling of the Krylov subspace, such as the precise values of the hopping parameters, still requires the same computational costs as ED, yet when the operator of interest has some universal features, the Krylov subspace can have some general properties. For example, the Krylov subspace of maximally chaotic systems have certain universal features much discussed in the literature [37–40].

In this paper we showed that when the operators are strong modes or almost strong modes, they appear as stable or quasi-stable edge modes of Krylov subspaces with topological properties. For the examples studied in this paper, the Krylov subspaces are given by generalized SSH models with long range and spatially inhomogeneous hopping. Exploiting these topological structures can lead to better understanding of the long lifetimes of the almost strong modes.

Most studies on Krylov subspace dynamics use the Lanczos method where the generator of dynamics is a

static Hamiltonian [36–40]. In studying Floquet systems, as we do in this paper, one has to adapt the Krylov subspace because the generator of dynamics is a unitary operator rather than a Hermitian operator. This led us to derive the Krylov subspace using an alternate approach, known as the the Arnoldi iteration [31]. Topological features of the resulting chain were highlighted. A compact expression (c.f. Eq. (77)) for the lifetime of the edge modes was derived and compared with ED. In particular, we showed that the decay rate is simply determined by the probability of finding the particle on the last site  $N$  of the  $W$  matrix that generates the time-evolution in this Krylov subspace. This observation opens up the possibility of developing analytic tools for calculating the decay rate, such as by employing the WKB approximation.

Our methods can be generalized to study other kinds of slow dynamics such as dynamics of scar states [42–45]. It is also promising to perform a topological classification of the Krylov subspaces of edge modes of strongly interacting topological insulators, both static and Floquet [46–48].

*Acknowledgements:* The authors thank Sasha Abanov for helpful discussions. This work was supported by the US Department of Energy, Office of Science, Basic Energy Sciences, under Award No. DE-SC0010821.

- 
- [1] A. Y. Kitaev, Unpaired majorana fermions in quantum wires, *Physics-Uspekhi* **44**, 131 (2001).
- [2] S. Sachdev, *Quantum Phase Transitions*, Cambridge University Press (2011).
- [3] B. A. Bernevig and (with T. L. Hughes), *Topological Insulator and Topological Superconductors*, Princeton University Press, Princeton (2013).
- [4] A. Kitaev, Anyons in an exactly solved model and beyond, *Annals of Physics* **321**, 2 (2006), january Special Issue.
- [5] C. Nayak, S. H. Simon, A. Stern, M. Freedman, and S. Das Sarma, Non-abelian anyons and topological quantum computation, *Rev. Mod. Phys.* **80**, 1083 (2008).
- [6] J. Alicea, New directions in the pursuit of majorana fermions in solid state systems, *Reports on Progress in Physics* **75**, 076501 (2012).
- [7] S. D. Sarma, M. Freedman, and C. Nayak, Majorana zero modes and topological quantum computation, *njp Quantum Information* **1**, 15001 (2015).
- [8] K. Sacha and J. Zakrzewski, Time crystals: a review, *Reports on Progress in Physics* **81**, 016401 (2017).
- [9] D. V. Else, C. Monroe, C. Nayak, and N. Y. Yao, Discrete time crystals, *Annual Review of Condensed Matter Physics* **11**, 467 (2020).
- [10] V. Khemani, R. Moessner, and S. Sondhi, A brief history of time crystals, arXiv:1910.10745 (2019).
- [11] P. Fendley, Strong zero modes and eigenstate phase transitions in the xyz/interacting majorana chain, *Journal of Physics A: Mathematical and Theoretical* **49**, 30LT01 (2016).
- [12] D. V. Else, P. Fendley, J. Kemp, and C. Nayak, Prethermal strong zero modes and topological qubits, *Phys. Rev. X* **7**, 041062 (2017).
- [13] J. Kemp, N. Y. Yao, C. R. Laumann, and P. Fendley, Long coherence times for edge spins, *Journal of Statistical Mechanics: Theory and Experiment* **2017**, 063105 (2017).
- [14] D. E. Parker, R. Vasseur, and T. Scaffidi, Topologically protected long edge coherence times in symmetry-broken phases, *Phys. Rev. Lett.* **122**, 240605 (2019).
- [15] J. Kemp, N. Y. Yao, and C. R. Laumann, Symmetry-enhanced boundary qubits at infinite temperature, *Phys. Rev. Lett.* **125**, 200506 (2020).
- [16] D. J. Yates, A. G. Abanov, and A. Mitra, Lifetime of almost strong edge-mode operators in one-dimensional, interacting, symmetry protected topological phases, *Phys. Rev. Lett.* **124**, 206803 (2020).
- [17] D. J. Yates, A. G. Abanov, and A. Mitra, Dynamics of almost strong edge modes in spin chains away from integrability, *Phys. Rev. B* **102**, 195419 (2020).
- [18] L. Jiang, T. Kitagawa, J. Alicea, A. R. Akhmerov, D. Pekker, G. Refael, J. I. Cirac, E. Demler, M. D. Lukin, and P. Zoller, Majorana fermions in equilibrium and in driven cold-atom quantum wires, *Phys. Rev. Lett.* **106**, 220402 (2011).
- [19] V. M. Bastidas, C. Emary, G. Schaller, and T. Brandes, Nonequilibrium quantum phase transitions in the ising model, *Phys. Rev. A* **86**, 063627 (2012).
- [20] M. Thakurathi, A. A. Patel, D. Sen, and A. Dutta, Floquet generation of majorana end modes and topological invariants, *Phys. Rev. B* **88**, 155133 (2013).
- [21] J. K. Asbóth, B. Tarasinski, and P. Delplace, Chiral sym-

- metry and bulk-boundary correspondence in periodically driven one-dimensional systems, *Phys. Rev. B* **90**, 125143 (2014).
- [22] D. J. Yates, F. H. L. Essler, and A. Mitra, Almost strong  $(0, \pi)$  edge modes in clean interacting one-dimensional floquet systems, *Phys. Rev. B* **99**, 205419 (2019).
- [23] V. Khemani, A. Lazarides, R. Moessner, and S. L. Sondhi, Phase structure of driven quantum systems, *Phys. Rev. Lett.* **116**, 250401 (2016).
- [24] C. W. von Keyserlingk, V. Khemani, and S. L. Sondhi, Absolute stability and spatiotemporal long-range order in floquet systems, *Phys. Rev. B* **94**, 085112 (2016).
- [25] C. W. von Keyserlingk and S. L. Sondhi, Phase structure of one-dimensional interacting floquet systems. i. abelian symmetry-protected topological phases, *Phys. Rev. B* **93**, 245145 (2016).
- [26] C. W. von Keyserlingk and S. L. Sondhi, Phase structure of one-dimensional interacting floquet systems. ii. symmetry-broken phases, *Phys. Rev. B* **93**, 245146 (2016).
- [27] H. Katsura, D. Schuricht, and M. Takahashi, Exact ground states and topological order in interacting kitaev/majorana chains, *Phys. Rev. B* **92**, 115137 (2015).
- [28] J. Wouters, H. Katsura, and D. Schuricht, Exact ground states for interacting kitaev chains, *Phys. Rev. B* **98**, 155119 (2018).
- [29] K. Wada, T. Sugimoto, and T. Tohyama, Coexistence of strong and weak majorana zero modes in an anisotropic xy spin chain with second-neighbor interactions, *Phys. Rev. B* **104**, 075119 (2021).
- [30] D. J. Yates, A. G. Abanov, and A. Mitra, Long-lived  $\pi$  edge modes of interacting and disorder-free floquet spin chains, arXiv:2021.13766 (2021).
- [31] W. E. Arnoldi, The principle of minimized iterations in the solution of the matrix eigenvalue problem, *Quart. Appl. Math.* **9**, 17 (1951).
- [32] T. Prosen, Exact time-correlation functions of quantum ising chain in a kicking transversal magnetic field: Spectral analysis of the adjoint propagator in heisenberg picture, *Progress of Theoretical Physics Supplement* **139** (2000).
- [33] V. Gritsev and A. Polkovnikov, Integrable Floquet dynamics, *SciPost Phys.* **2**, 021 (2017).
- [34] W. P. Su, J. R. Schrieffer, and A. J. Heeger, Solitons in polyacetylene, *Phys. Rev. Lett.* **42**, 1698 (1979).
- [35] W. P. Su, J. R. Schrieffer, and A. J. Heeger, Soliton excitations in polyacetylene, *Phys. Rev. B* **22**, 2099 (1980).
- [36] V. Vishwanath and G. Müller, *The Recursion Method: Applications to Many-Body Dynamics*, Springer, New York (2008).
- [37] D. E. Parker, X. Cao, A. Avdoshkin, T. Scaffidi, and E. Altman, A universal operator growth hypothesis, *Phys. Rev. X* **9**, 041017 (2019).
- [38] A. Dymarsky and A. Gorsky, Quantum chaos as delocalization in krylov space, *Phys. Rev. B* **102**, 085137 (2020).
- [39] J. Barbón, E. Rabinovici, R. Shir, and R. Sinha, On the evolution of operator complexity beyond scrambling, *Journal of High Energy Physics* **2019**, 264 (2019).
- [40] A. Avdoshkin and A. Dymarsky, Euclidean operator growth and quantum chaos, *Phys. Rev. Research* **2**, 043234 (2020).
- [41] R. A. Horn and C. R. Johnson, *Matrix Analysis*, Cambridge University Press, 2nd Edition (2013).
- [42] S. Moudgalya, E. O'Brien, B. A. Bernevig, P. Fendley, and N. Regnault, Large classes of quantum scarred hamiltonians from matrix product states, *Phys. Rev. B* **102**, 085120 (2020).
- [43] C. J. Turner, A. A. Michailidis, D. A. Abanin, M. Serbyn, and Z. Papić, Weak ergodicity breaking from quantum many-body scars, *Nature Physics* **14**, 745 (2018).
- [44] W. W. Ho, S. Choi, H. Pichler, and M. D. Lukin, Periodic orbits, entanglement, and quantum many-body scars in constrained models: Matrix product state approach, *Phys. Rev. Lett.* **122**, 040603 (2019).
- [45] C.-J. Lin and O. I. Motrunich, Exact quantum many-body scar states in the rydberg-blockaded atom chain, *Phys. Rev. Lett.* **122**, 173401 (2019).
- [46] L. Fidkowski and A. Kitaev, Effects of interactions on the topological classification of free fermion systems, *Phys. Rev. B* **81**, 134509 (2010).
- [47] A. C. Potter, T. Morimoto, and A. Vishwanath, Classification of interacting topological floquet phases in one dimension, *Phys. Rev. X* **6**, 041001 (2016).
- [48] D. V. Else and C. Nayak, Classification of topological phases in periodically driven interacting systems, *Phys. Rev. B* **93**, 201103 (2016).